A Binder-Free Electrocatalytic Cathode for Lithium Oxygen Batteries

by
Jerome Fineman

A thesis submitted to Johns Hopkins University in conformity with the requirements for the degree of Master of Science

Baltimore, Maryland
May, 2016

Abstract

Lithium oxygen (Li-O_2) batteries have promising potential as a next generation energy storage technology due to their high specific energy density of 3500 Wh/kg. However, Li-O_2 batteries are still in early development and there are many challenges and problems that need to be solved before commercialization. Two of the most critical issues hindering Li-O_2 battery performance are cyclability and round trip efficiency, both of which are dependent on the oxygen reduction reaction (ORR) and oxygen evolution reaction (OER). The slow kinetics of these reactions translate to large over potentials during cycling. Adding electrocatalysts to the cathode has shown to significantly enhance the activity for ORR and OER during discharge and charge, significantly increasing the performance of Li-O_2 batteries. Thus, the development of a binder free electrocatalytic cathode was proposed for this master thesis. This research investigated the use of a bi-functional α-MnO2 nanowire catalyst with a carbon nanotube (CNT) conductive support as a cathode for sealed Li-O2 batteries. The air cathode was constructed by vacuum filtering a 70/30 wt% α-MnO_2/CNT mixture onto glass fiber filter paper. Electrochemical studies were conducted to evaluate the performance of the cathodes. In addition, postmortem analyses were done using scanning electron microscopy and x-ray diffraction. The results of this research showed that the binder free construction proved to be a viable cathode for Li-O_2 batteries. Stable cycling was achieved with a capacity of 500 mAh/$g_{cathode}$ on discharge and charge for >50 cycles. Postmortem analyses of the batteries revealed that pore clogging by irreversible and unfavorable discharge products is the most likely mode of failure. Lastly, the facile method developed to construct the cathode is highly tunable, which allows for the future addition of other catalysts.

Acknowledgments

This thesis is dedicated to my wife, who's undying support and encouragement drove me to be where I am today. I can't wait for the adventures we have ahead of us.

I would like to thank my advisor Professor Chao Wang for his guidance throughout my tenure in his lab. He continually pushed me to think critically about my research, but gave guidance and advice when I needed it. I would also like to thank Dr. Lei Wang for helping me develop an experimental plan and for his constant wealth of knowledge about Li-ion and Li-air batteries. Without the guidance from Chao and Lei, this work would not have been possible.

I would also like to thank Matt Gonzalez. He collaborated with me on this project. It was our collective efforts that drove this project to completion. Working together was a pleasure. We worked hard, but were able to have fun at the same time. I am particularly grateful for his help with SEM, he always was able to resolve much better images then I ever had.

Lastly I would like to thank the rest of the members of the Wang lab. We were a rag tag group that always had the support of one another. The collaborative nature of the group drives the strong scientific discoveries that happen every day.

Table of Contents

List of Figures

Chapter 1: Introduction

1.1 Motivation

Rapid climate change and warming of the planet over the past century has made the curb of green house gasses imperative. The scientific consensus of a $2^{O}C$ increase in average global temperature will cause damaging and irreversible climate change. Recently, the Paris Climate Agreement, which was negotiated in December 2015, solidified an international agreement to peak global emissions as soon as possible, and to reduce emissions soon after in an effort to mitigate the decades of pollution from the use of fossil fuels.[1]

Nearly one third of all greenhouse gasses are produced by the energy and transportation sectors, which produce >90% of their energy from fossil fuels.[2] Therefore, a cleaner and more sustainable future has to include renewable energy sources (wind, solar, and tidal energy) and fossil fuel free transpiration such as electric vehicles (EVs). However, due to the intermittent nature and geographical limitations of each power source, and the range requirements for transportation, reliable energy storage is needed to achieve these goals. According to market research firm IHS , annual global energy storage installation will "explode" from 6 GW in 2017 to 40 GW by 2020,[3] creating a $55 billion lithium battery market at the same time.[4]

Though adoption of electric vehicles has seen significant growth over the last few years, limited driving range and high battery costs have limited EV's market share of

consumer transportation. Current state of the art electric vehicles use lithium-ion (Li-Ion) batteries due to their relatively long cycle life and high-energy efficiency. However, due to their chemical "rocking chair" mechanism, future generations of Li-Ion batteries are limited to a theoretical energy density of ~400 Wh kg.[1] This would translate to a range of about 200km per charge, which is far below the range of an internal combustion vehicle of the same size. To meet the demands of the consumers, development of new battery technologies must reach beyond the limitations for Li-Ion and deliver batteries with energy densities comparable to fuels for internal combustion engines. There are a few technologies under development that, once commercialized, would far surpass these requirements. Zinc-air (Zn-air),[5] Lithium-air (Li-air) and Lithium-Sulfur (Li-S) batteries have gained considerable interest due to their high energy densities and range capabilities.[6] Figure 1 shows the practical specific energy for different battery chemistries and the estimated driving range based of the pack weight for the Nissan Leaf, a fully electric vehicle. Though still in the research and development phase, Li-air batteries show the greatest potential with an estimated driving of >550 km (~340 miles), putting it on par with internal combustion engines.

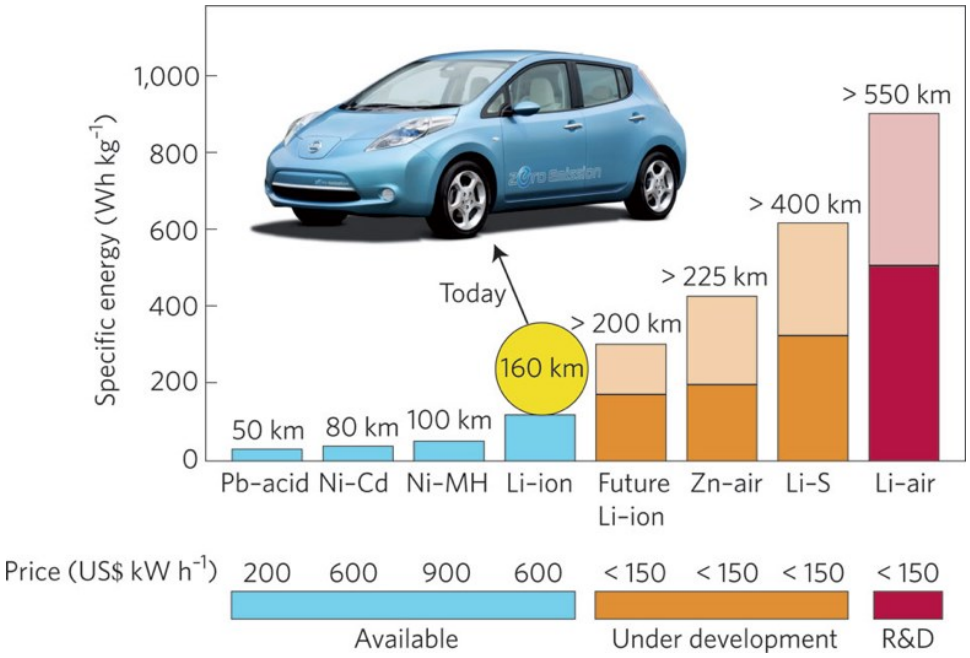

Figure 1: Practical specific energies for some rechargeable batteries, along with estimated driving distances and pack prices. For future technologies anticipated range is shown by lighter shade region of the bar. The values are scaled against the specific energy of Li-Ion cell and driving range of a Nissan Leaf.[6]

1.2 The Lithium Oxygen Battery

1.2.1 Introduction to the Li-O_2 Battery

Though generally referred to as Li-air battery, Li-O_2 is a commonly used and more accurate name due to O_2's role as the reactive species in air. The first Li-O_2 battery prototype was introduced in 1996;[7] however, it was not until a decade later that Bruce et al. revisited the battery creating the massive interest we see today.[8] Li-O_2 batteries, are fundamentally different then lithium ion in that there is not intercalation of lithium into the electrode; rather, the lithium ion reacts with dissolved oxygen at the cathode, creating Li-Oxygen discharge products. The theoretical specific energy of a Li-O_2 battery is reported as 11,586 Wh kg^{-1}; however, this is based solely on the capacity of Li metal and does not take in to account the increase in weight from the atmospheric O_2 that enters the electrode during discharged. If including the weight of the discharge products, the theoretical capacity of a Li-O_2 battery should 3,505 Wh kg^{-1}.[9]

Currently four architects for Li-O2 batteries are being developed each using a different form of electrolyte: aprotic, aqueous, solid state, and mixed aqueous/aprotic (Figure 2).[10] Aprotic, aqueous, and mixed architectures all employ liquid electrolytes, while the electrolyte for the solid-state architecture is composed of polymer and glass ceramics. Aprotic cells have the advantage, over aqueous and mixed electrolyte architectures, of the Li metal anode being in direct contact with the electrolyte. Aqueous and mixed electrolytes must employ a Li^+ permeable membrane between the anode and aqueous electrolyte to prevent water from reacting with Lithium metal. It's for this reason that the scope of my thesis will cover Li-O2 cells using aprotic electrolytes.

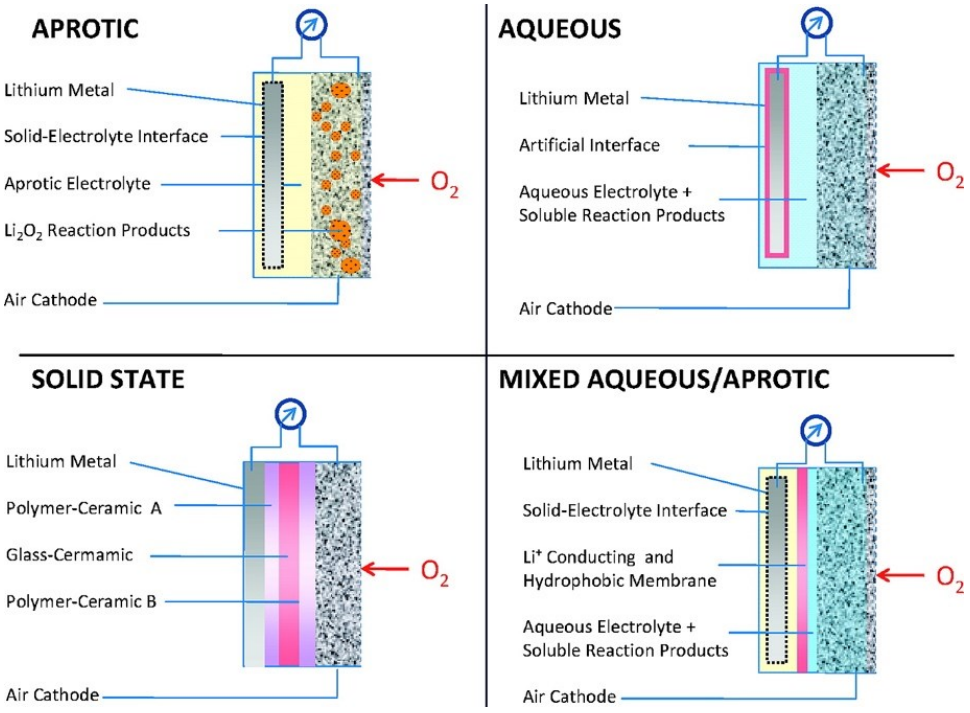

Figure 2: Four different architectures of Li–air batteries, which all assume the use of lithium metal as the anode. The three liquid electrolyte architectures are aprotic, aqueous, and a mixed aprotic–aqueous system. In addition, a fully solid state architecture is also given. Principal components are as labeled in the figure. Spontaneously occurring SEIs on the lithium anode are given as dashed lines, while artificial SEIs are given as solid lines.[10]

1.2.2 Reaction Mechanisms for Li-O_2 Batteries in Aprotic Electrolytes

Figure 4 for shows a schematic of the operating principles during charge and discharge in an aprotic Li-O_2 cell.[11] During charge and discharge, the lithium-metal anode undergoes plating and stripping reactions. During the discharge (stripping), the metal anode is oxidized, releasing Li^+ into the electrolyte solution. On charge this process is reversed and the Li^+ is reduced, re-plating on the metal anode. At the cathode, O_2 from the atmosphere enters the porous electrode, where it dissolves into the electrolyte. During discharge the dissolved oxygen is reduced at the electrode surface (oxygen reduction reaction, ORR) reacting with Li^+ forming an Li_xO_2 species on the air electrode surface. During charge, the Li_xO_2 is oxidized regenerating the gas, releasing it into the atmosphere.

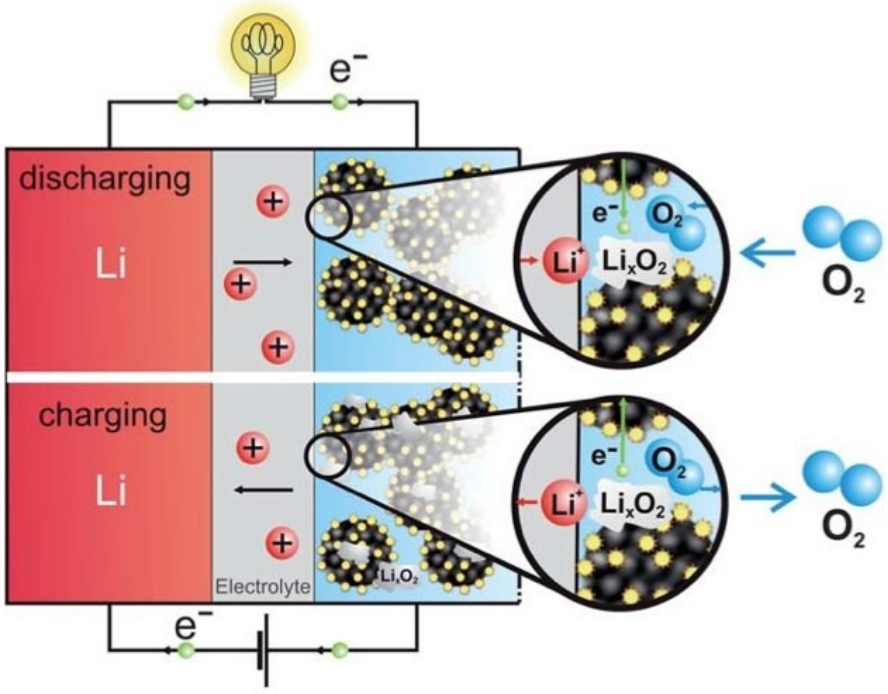

Figure 3: Schematic of operating principle of Li-O_2 cell during charge and discharge. On discharge Li^+ ions move across the electrolyte reacting with dissolved O_2 at the cathode surface forming Li_xO_2 species. On charge Li_xO_2 is oxidized, where Li^+ ion travels back across the electrolyte and the O_2 is reformed.[11]

As discussed by Laoire *et al. (2010)* the reduction of oxygen can follow a complex set of reaction mechanisms, potentially forming three different oxygen compounds: oxides, superoxides, and peroxides. The formation of each of these species from the reaction between O_2 and Li, as well as their theoretical voltages, are described below[12].

Lithium Peroxide:

$$2Li + O_2 = Li_2O_2 \qquad \Delta G^0 = -145 \text{ kcal } (E^0 = 3.1 \text{ V}) \qquad (1)$$

Lithium Oxide:

$$4Li + O_2 = 2Li_2O \qquad \Delta G^0 = -268 \text{ kcal } (E^0 = 2.91 \text{ V}) \qquad (2)$$

Lithium Superoxide:

$$Li + O_2 = LiO_2 \qquad \Delta G^0 = -70 \text{ kcal } (E^0 = 3.0 \text{ V}) \qquad (3)$$

The consensus from the scientific community, which is well documented in the literature, is that the primary discharge products are Li_2O_2 and LiO_2.[6,12-14] Equation 1 and 2 are both direct reductions with the former undergoing a $2e^-$ reduction to a peroxide species and the later undergoing a $4e^-$ reduction to an oxide species. Laoire *et al.* showed that the formation of the superoxide, as shown in equation 3, is highly unstable in the presence of Li^+ ions and proposed that the LiO_2 is actually an intermediate composition that either disproportionates or is further reduced to Li_2O_2. *Peng et al.* confirmed the mechanism using surface enhanced Ramen Spectroscopy.[15] This mechanism is described in the following scheme[14] and equations.[12]

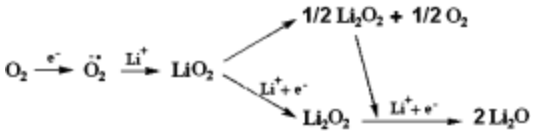

Figure 4: Scheme of oxygen-molecule reduction in aprotic systems.[14]

$$O_2 + Li^+ + e^- = LiO_2 \quad \text{(Electrochemical)} \qquad (4)$$

$$LiO_2 + Li^+ + e^- = Li_2O_2 \text{ (Electrochemical)} \qquad (5)$$

$$2\ LiO_2 = Li_2O_2 + O_2 \quad \text{(Chemical)} \qquad (6)$$

As depicted in Figure 4 and equations 4, 5 and 6, the dissolved Oxygen is reduced at the electrode surface forming a superoxide where it reacts with a Li^+ from the electrolyte further forming the LiO_2 (Equation 1). The LiO_2 can then form the peroxide from 2 possible pathways. One pathway is electrochemical (equation 5) where the superoxide is further reduced and reacts with another Li^+ creating the peroxide species. On the other had, the superoxide can go through a disproportionation reaction creating Li_2O_2 and O_2. It has been proposed that Li_2O forms from further reduction of the Li_2O_2 at low potentials, but there has been little evidence of this so far.[6]

The process on charging does not follow the reverse of discharge, rather it follows the following direct decomposition pathway:

$$LiO_2 \text{ ® } 2Li^+ + 2e^- + O_2 \qquad (7)$$

Discharge involves the formation of superoxide as an intermediate where as on discharge no intermediates are formed. This arises from the kinetics of oxidizing LiO_2 directly being faster then reversing the three steps on reduction, especially the disproportionation step.[6,15]

1.2.3 The Lithium Metal Electrode (Anode)

Low specific capacity of intercalation based anodes are acceptable for Li-ion batteries due to their high weight cathodes and electrolyte dominating the overall mass and energy density. However, the low weight of the Li-O_2 cathode demands a much more energy dense anode. With an energy density of 3862 mAh/g_{Li} a lithium metal anode can afford the capacity requirements of the air cathode[16]. During discharge, the anode is oxidized releasing Li^+ to the electrolyte providing ionic conduction where it will react with reduced oxygen at the cathode surface forming LiO_2.

While the high energy density of the lithium metal makes it an attractive anode, there are safety concerns that have made international headlines. Dendrites, the major cause for concern, can cause shorts that vigorously react with the contaminates in the batteries creating thermal runaways and fires.[10] When lithium metal is placed in an organic electrolyte, an immediate and spontaneous formation of a conductive Li-ion thin film occurs at the interface creating a corrosion resistant lithium salt barrier, known as the solid electrolyte interface (SEI);[17] schematically drawn in Figure 5. The Li anode goes through stripping and plating during cycling of the battery causing defects in the brittle nature of the SEI. During plating, non-uniform deposition caused by uneven current

distribution at the metal-electrolyte interface will create preferential deposition of lithium metal forming dendrites and moss. However, the presence of Li^+ is required for the reaction. Thus, the commercialization of the Li-O_2 battery must address these safety concerns prior to mass production.

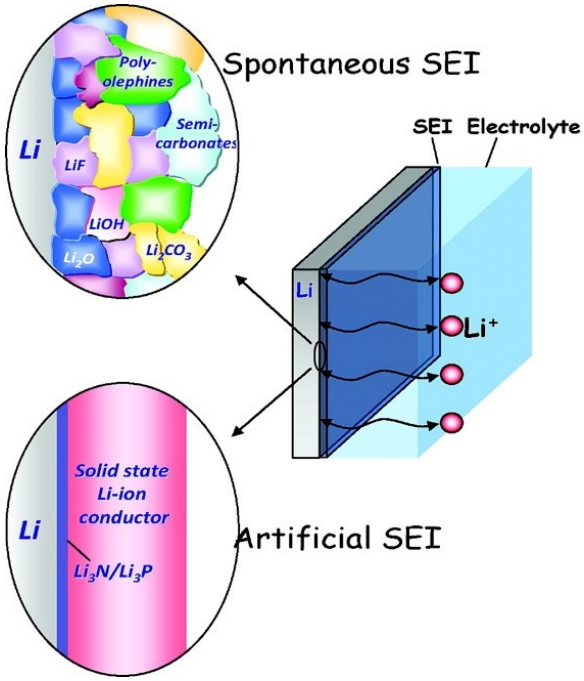

Figure 5: Schematic drawing of the lithium metal−electrolyte interface choices. Both the complicated natural SEI formed by reduction of the electrolyte and an artificial SEI, e.g., Li-ion-conducting ceramic, are shown as examples.[10]

1.2.4 Electrolyte

Fundamentally, a battery must have a layer that isolates the cathode from the anode to prevent shorting. The key properties of this layer is it must be electrically insulating, yet ion conducting to allow the electrochemical circuit to be created. In liquid electrolyte based batteries, this layer is generally composed of a salt, solvent, and porous insulating membrane. The salt and solvent in the electrolyte serve as an ionic interconnection between the anode and cathode, essential for the movement of charge between the two electrodes and balancing the electron movement though the external circuit. In Li-O_2 cells the electrolyte is a key component, and one of the main challenges to a functioning battery. A successful electrolyte must have the following properties:[6] stable to O_2 and it's reduced species as well as Lithium-oxygen species that form on discharge; high O_2 solubility and diffusion; high Li^+ conductivity; high wetting of electrode surfaces; and low volatility to avoid evaporation. Reversible formation/decomposition of Li_2O_2 at the cathode, as well as the decomposition of the electrolyte serve as major problems in the electrolyte, effecting the reaction kinetics, cyclibility and calendar life of the battery. Early Li-O_2 batteries employed carbonate based electrolytes, due to their low volatility, high oxidative stability, and abundant use in Li-ion batteries; however recent research has shown that organic carbonate electrolytes are unstable in this cell with little evidence of peroxide formation occurring.[9,15,18-21] Thus finding new stable aprotic electrolytes is presently the subject of much research. The next generation of aprotic electrolytes under investigation can be categorized into those based on ethers, amides, ionic liquids, sulfonates and dimtethyl sulfoxide (DMSO). These

electrolytes have been identified as predominately promoting the formation and decomposition of Li_2O_2 on charge and discharge.[22]

Ether-Based Electrolytes

Once the instability and decomposition of carbonate in Li-O_2 cells was discovered, research pivoted towards electrolytes based on ethers.[14,19,22-24] Ether based electrolytes, such as tetraethylene glycol dimethyl ether (TEGDME) and dimethoxyethane (DME), possess many of the features previously stated: they are compatible with the Li metal anode, are stable at high voltages (4V vs Li/Li^+), and low volatility for high molecular weight ethers. More critically, they were also expected to be highly resistant to nucleophilic attack and decomposition by reduced O_2 species. However despite promise, recent experimental and theoretical work has concluded otherwise.[19,20,22,23] Experiments have shown that Li_2O_2 is the predominate discharge product; however, it was also shown that significant decomposition occurs forming a variety of lithium containing carbonaceous species such as Li-Carbonate and polyethers/esters. Though initial theories were promising, ether based electrolytes, including TEGDME and DME, proved to be unstable in a secondary cell. The decomposition, leading to significant formation of Li_2CO_3, results in significant capacity fade after the first cycle[22].

Ionic-Liquid-Based Electrolytes

Though ionic liquids (IL) have been used for some time in O_2 reduction studies, they have only recently been employed for testing in Li-O_2 cells. Room temperatures ILs have advantages over traditional nonaqueous electrolytes, such as negligible volatility, high ionic conductivity, nonflammable, can be designed to be hydrophobic, and are stable in large voltage windows.[25] Shown below, Figure 6 illustrates possible candidates, with the most promising ILs being of the piperidimium, imidazolium and pyrroliidinium forms. Initial studies have shown that ILs stability is significantly improved over organic carbonate solvents, with Li_2O_2 being the predominant component on 1st discharge.[26] However, a small fraction of carbonates are formed during cycling leading to a decrease in capacity and a retention of 20% of the capacity by the 20th cycle.[27] Ionic liquids still show great potential as an electrolyte solvent due to their resistance to evaporation and reported stability. However, the loss of capacity in cycling suggest side reactions do occur; thus, further studies must be performed to determine if the Li_2CO_3 is formed through decomposition of the electrolyte or by the instability of the carbon air electrode.

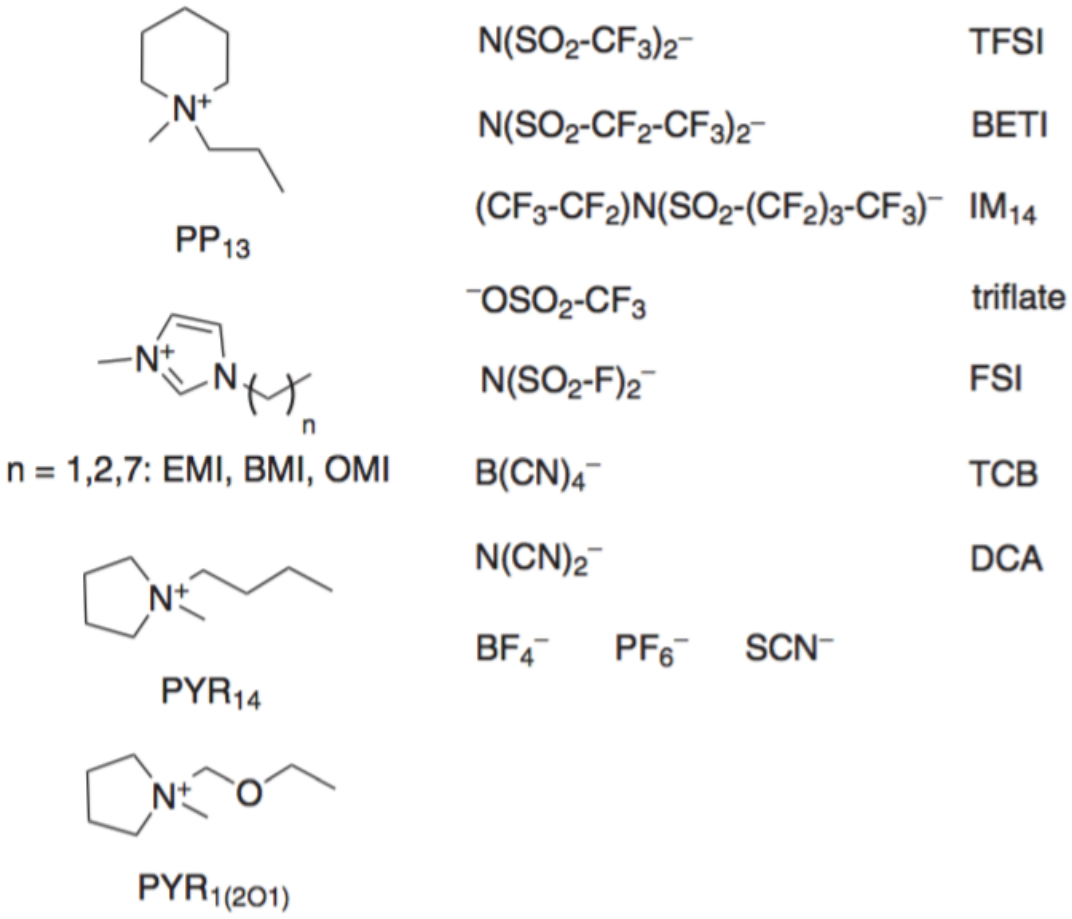

Figure 6: Overview of Ionic Liquids studied so far for LI-O_2 battery applications. Various combinations of depicted cations and anions were used.[9]

Amide-Based Electrolytes

Amide-based electrolytes such as dimethylformamide (DMF), dimethylacetamide (DMA) and N-methyl-2-pyrrolidone (NMP) garnered significant attention due to their high stability against nucleophilic attack and auto-oxidation. However, studies performed by Chen Y. *et al.* demonstrated that significant capacity fade does occur during cycling as well as the charge plateau shifting to higher voltages.[28] These results were a clear indication of side reactions. To verify the origins of the side reactions, the carbon

electrode was replaced with nanoporous gold (NPG). The side reactions were still observed, elucidating the formations originated from the decomposition of the amide-based solvents.

Dimethyl Sulfoxide-Based Electrolytes

Dimethyl sulfoxide (DMSO) has demonstrated high cycle life with the predominant, efficient, and reversible formation of lithium Li_2O_2 at the cathode.[12] Peng Z. *et al.* demonstrated that using DMSO as an electrolyte with a NPG electrode, instead of one that is carbon based, was able to retain 95% of its capacity after 100 cycles.[29] FTIR and other spectrographic techniques were employed to confirm that Li_2O_2 was the main discharge product and that carbonates accounted for <1% of products form on each cycle. It's important to note they while DMSO has shown do be extremely stable as an electrolyte solvent with NPG, it does decompose at voltage greater then 4V, however, for an Li-O_2 battery must charge below this threshold to be commercially viable.

Electrolyte Salts

Electrolyte salts play a pivotal role in Li-O_2 batteries. Not only do they provide the needed ionic conductivity, but are crucial in the formation and stability of the SEI. Once again taking for Li-Ion batteries, lithium hexaflourophosphate ($LiPF_6$) was the first candidate for use in Li-O_2 batteries and is still the most widely used. More recently investigation in other salts, among others, include: $LiClO_4$, $LiBF_4$, Li Imides such as Bis(trifluoromethane)sulfonimide (TFSI).[30] Like solvents, the stability for the salts against O_2^- is mandatory for extended cycle life. Nasybulin *et al.* studied the stability of

various salts in TEGDME. [30] From their experiments they found LiTFSI and LiTF to be the most stable, providing the highest capacity after first cycle and highest capacity retention after 20 cycles.

The stability of nonaqueous electrolytes for use in Li-O_2 batteries garnered much scientific attention once it was realized that carbonate solvents are highly susceptible to nucleophilic attack by O_2^- and LiO_2 causing decomposition and irreversible carbonate formation. A range of second generation electrolytes based on ethers, amides, ILs and DMSO, as well Li-Salts have been investigated for stability in the system. Though all show higher resistance to decomposition then their carbonate based predecessors, carbon based electrodes proved to be a large source of instability in the electrolytes causing decomposition and carbonate formations.[31]

1.2.5 The Air Electrode (Cathode)

Cathodes for Li-O_2 batteries are fundamentally different then those employed in Li-Ion batteries. Instead of an intercalation reaction, as in Li-Ion, discharge products, mainly Li_2O_2, are formed/decomposed at the electrode surface during cycling. Thus the requirements for an air cathode are fundamentally different as well. An ideal cathode should have the following properties: offer transport channels for fast oxygen diffusion; provide a three phase (electrolyte/cathode/oxygen) interphase; and adequate void space for the formation of discharge products. Figure 7, shown below, depicts a schematic representation of an ideal air cathode exhibiting the previous requirements. Construction of air cathodes generally include a mixture of catalyst (to increase ORR/OER activity),

carbon (for high surface area substrate and gas diffusion), a porous current collector, and binder. However, this construction paradigm lacks the previously stated requirements. Thus, significant work has been conducted in the search for novel cathode designs and materials.

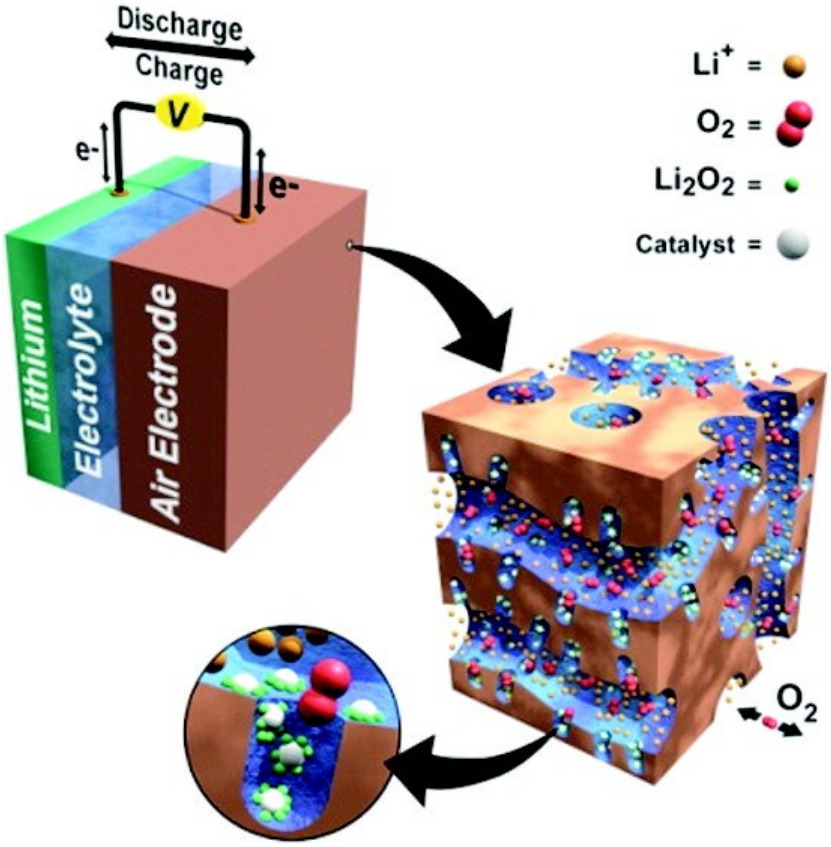

Figure 7: Schematic representation of air electrode, including electrocatalysts, reactants (O_2 and Li^+), and discharge products (Li_2O_2), exhibiting ideal requirements for an Li-O_2 battery.[32]

Carbon-Based Air Cathodes

Though not technically an electrocatalyst, porous carbon is the most widely used material for air cathodes due to it's high surface area, high electrical conductivity, and low cost. In addition, carbon's high porosity is vital as a gas diffusion electrode (GDE); it provides the fast transport of O_2 needed during discharge and adequate pore space to accommodate the discharge products. Studies performed by Tran *et al.* demonstrated that larger mesopores could accommodate more discharge products than its smaller counter part, which more readily get clogged.[33] This discovery highlighted the need to optimize pore size for increased performance and cycle life. One dimensional (1-D) carbon materials such as carbon nanotubes (CNT) and carbon fibers/nanofibers have been investigated as a porous GDEs in Li-O_2 batteries. A major advantage of 1-D carbon materials is the ability to form freestanding structures allowing the electrodes to be constructed with out the nonconductive organic binders, leading to closer packing and increased cycle life.[34,35]

The slow kinetics of the OER and ORR reactions cause large overpotentials during cycling of Li-O_2 batteries, thus the use of carbon-supported catalysts have been investigated to enhance the activity of the OER and ORR reaction. Numerous studies have shown that a wide range of catalysts, such as precious metals and metal oxides, are able to reduce the overpotentials due to OER/ORR. Research lead by Bruce et al. demonstrated the use of metal oxides, such as various phases of MnO_2,[36] Iron oxides, cobalt oxides, and others.[37] From their research they discovered MnO_2 nanowires have the best performance, showing the highest discharge capacity and cycle life, and lowest

charge plateau (highest activity). Studies of precious metals for catalysts in Li-O_2 batteries were performed by Shao-Horn et. al.[24,38] Through their investigations they discovered that Au/C promotes the ORR process on discharge, while Pt/C promotes OER on charge. Once this discovery was made, a bifunctional catalyst was made from a Pt-Au alloy which significantly reduced the over potentials on cycling increasing the round trip efficiency from 57% to 73%.[38]

Carbon-based air electrodes show great promise as GDEs due to their close packing and large mesoporous structure; however, carbon based electrodes have been shown to enhance the instability of non-aqueous electrolytes. An in depth study, by Ottakam *et al.,* on carbon-based electrodes, shows the carbon promotes decomposition of electrolyte on discharge leading to side reaction formation of Li_2CO_3 and lithium carboxolates.[31]

Non-Carbon-Based Air Cathodes

As discussed above, carbon based electrodes have been shown to increase electrolyte decomposition leading to the formation of irreversible discharge products; thus, the need for non-carbon based electrodes. Work by Bruce *et al.* has investigated two new kinds of electrodes; nanopourous gold (NPG)[29], and TiC.[39] NPG was employed as a cathode to increase the stability of DMSO based electrolytes during cycling. This combination showed significant performance enhancement, stably cycling over 100 times while retaining 95% of its discharge capacity. However, the fabrication difficulty, and high price and mass of an all gold cathode make it impractical in Li-O_2 batteries. The

groups later discovery of a TiC cathode overcame the challenges and disadvantages of both carbon-based and NPG cathodes demonstrating 98% capacity retention after 100 cycles and minimal decomposition of the electrolyte.[39]

As with all other parts of the battery, the performance and stability of the air electrode has significantly improved since the battery was first discovered. However, greater understanding of the electrode must be made. To make the battery commercially viable fundamental understanding of the cathode reaction are needed to guide the development. In addition, newer and cheaper catalysts must be found to reduce the over potential on cycling. New cathode structures have been investigated showing great potential; however, they are only in the early stages of development.

1.2.6 Challenges Facing the Li-O_2 Battery

Lithium-Air batteries are considered to be the "Holy Grail" of battery technologies due to it's substantial increase specific energy over lithium-ion. However, from the previous sections it's evident that the Li-air battery is a very complicated system with each component hosting an array of challenges and difficulties (Figure 8) before it can be implemented for commercial applications. The main challenges that still face the current state of Li-O batteries are the high over potentials (low round-trip efficiency) due to the slow kinetics of the OER/ORR reactions, and instability/degradation of the aprotic electrolytes, which cause side reactions leading to poor reversibility and cycle life. It's now universally recognized that carbonate based electrolytes are highly unstable in the presence of O_2^- and LiO_2, and have thus been abandoned in favor of more stable

electrolytes, such as TEGDME, DMSO, and ILs. However, much research still needs to be performed to understand discharge products formed with these electrolytes. In addition, much work needs to focus on the air cathode, and specifically the use of catalysts and alternative electrode materials to increase the round trip efficiency and rate capabilities of the cell. The largest hurtle that must be overcome is the stability of the electrode in an ambient environment, not just pure O_2. The key difficulty here is isolating the electrochemical system from moisture in the air, as even trace amounts can lead to degradation of the lithium metal.

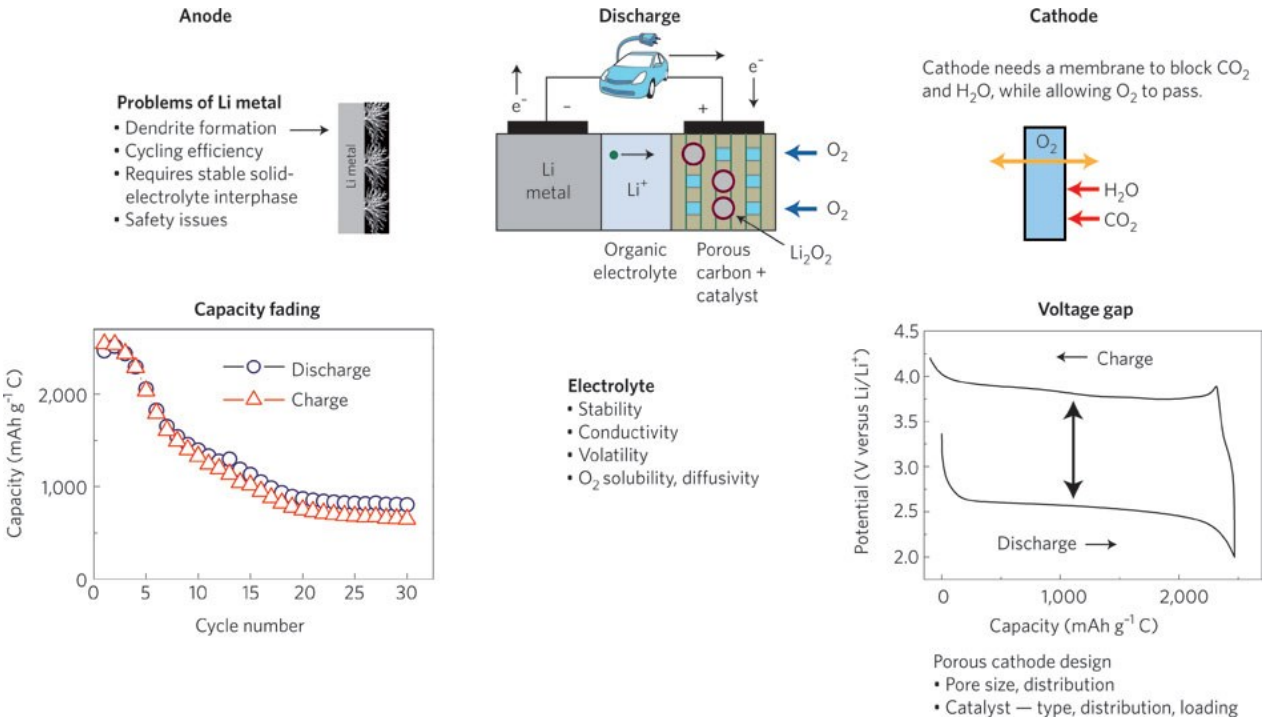

Figure 8: Challenges facing the non-aqueous Li–O_2 battery. Data illustrating capacity fading and the voltage gap were collected from a cell with an organic carbonate electrolyte, Li–1 M $LiPF_6$ in propylene carbonate–(superP:Kynar:α-MnO_2 nanowires). Use of more stable ether electrolytes and carbon fiber nanotube electrodes — for example, Li–$LiClO_4$ in dimethoxyethane–carbon fiber nanotube — reduces, although does not eliminate, capacity fading.[6]

Chapter 2: Electrocatalysts for Li-O_2

2.1: Introduction to Electrocatalysts

As discussed in the previous section on the air-cathode, enhancement of OER and ORR reaction kinetics with electrocatalyst have become a topic of great interest for reducing the overpotentials during cycling, thus increasing roundtrip efficiency of the battery. Shao-Horn et al. showed the use of precious metals, more specifically Au have a beneficial effect on the discharge (ORR) kinetics improving the discharge potential.[24] In addition, Bruce et al. demonstrated the beneficial effects of an α-MnO_2 nanowire bifunctional catalyst on capacity retention and cycle life. Our investigation into electrocatalysts set out to combine metal-oxide and precious metal electrocatalysts for increased ORR/OER activity in Li-O_2 batteries.

2.2: Electrocatalyst Synthesis

All particles were synthesized in-house using wet chemistry techniques. Using organic and aqueous solvent techniques allows for the synthesis of a wide range of tunable nanoparticles. To confirm the formation of the electrocatalysts, a series of characterization techniques were employed. Transmission electron microscopy (TEM) was performed on a 120kV, FEI Tecnai 12 Twin microscope. X-ray diffraction (XRD) patterns were collected on a PANalytical X'Pert^3 Powder X-Ray Diffractometer equipped with a Cu Kα radiation source (λ=0.15406). Scanning Electron Microscopy (SEM) was performed on a JEOL JSM-6700F Field Emission Scanning Electron Microscope capable of secondary electro imaging and back scattering.

2.2.1: Synthesis of Gold Nanoparticles

The syntheses of Au nanoparticles was adapted from the procedure by HIramatsu et al. in Chemistry of Materials.[40] In a typical synthesis 1.5 mL of Oleylamine, OAM, (70% laboratory grade, purchased from Sigma Aldrich) and 25 mL of toluene was brought to reflux in a three neck flask under a nitrogen atmosphere. Gold(III) chloride hydrate, $HAuCl_4$, (99.999%, purchased from Sigma Aldrich) dissolved in 0.6 mL of OAM and 0.5 mL of toluene was injected into the flask. The final solution was kept at reflux for 2 hours, turning from a clear/yellow to deep red. The solution was then brought to room temperature and diluted with ethanol. The Au nanoparticles were precipitated by centrifuge at 8000 RPM and dispersed in hexanes. Transmission electron spectroscopy (Figure 9) was used to determine the 0-d shape and ~15 nm size of the gold particles

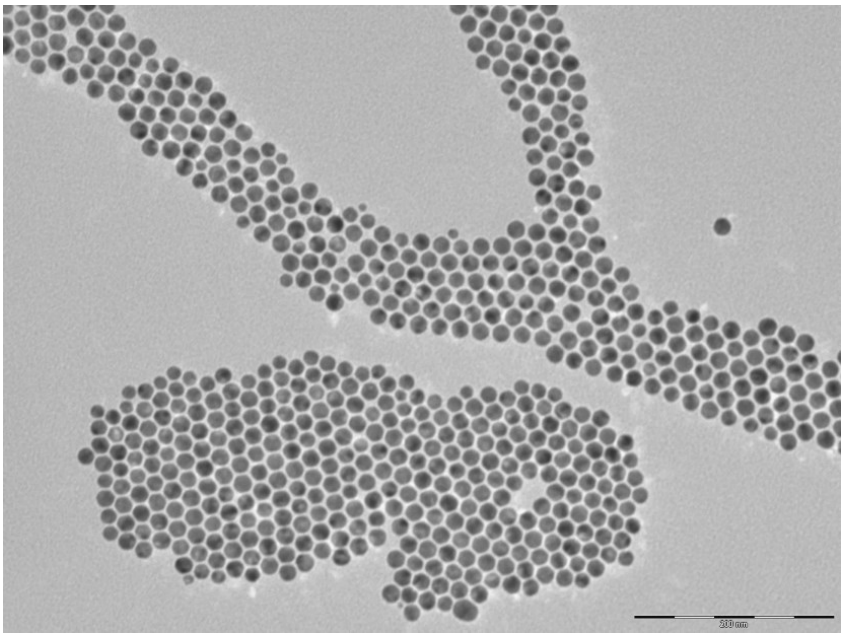

Figure 9: TEM micrograph of approx. 15 nm Au nanoparticles synthesized following procedure by Hiramatsy et al[40]. (scale bar represents 200 nm)

2.2.2 Syntheses of Gold Nanowires

The syntheses of Au nanowires followed the procedures reported by Kang *et al.*[41] In a typical synthesis 46 mg of AuCl (purchased from Sigma Aldrich) was dissolved in 20 ml of chloroform (purchased from Sigma Aldrich) and 1.84 ml of Olelyamin (70% laboratory grade, purchased from Sigma Aldrich) in a three neck flask. The mixture was then heated 60^{O}C and held for 10 min in a CO atmosphere. The solution was then cooled to room temperature and diluted with hexanes (purchased from Sigma Aldrich). The nanowires were precipitated by centrifugation at 6000 RPM and dispersed in hexanes.

The synthesis produced Au nanowires of 0.5 - 2 μm in length and <10nm In width (TEM images below). The wires have a very high aspect ratio and lots of kinks in their

structure. The wires formed webbed bundles when high concentrations were dropped on TEM grid as shown in Figure 10b.

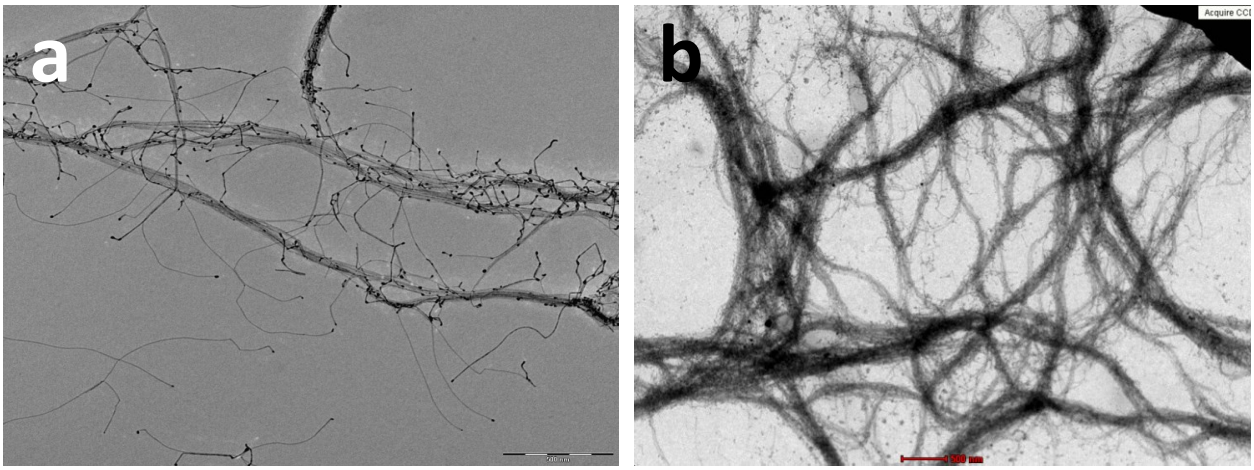

Figure 10 a-b: TEM images of Au nanowires, of 0.5 – 2 μm in length and < 10 nm in width, synthesized following procedure by Kang *et al.*[41] *(Scale bar represents 500 nm)*

2.2.3: Synthesis of α-MnO_2 Nanowires

The synthesis of the α-MnO_2 nanowires used for our tests followed the procedure by Sinha et al.[42] To synthesis the nanowires 4.74g of ACS grade potassium permanganate, $KMnO_4$, (purchased from Amresco) was dissolved in 150 ml DI water to form 20mM solution. 40 ml of ethyl acetate (purchased from Sigma Aldrich) and the aqueous solution were taken in a 500 ml round bottom flask forming a bi-phasic mixture. The mixture was refluxed at 85^{O}C until the purple color of the $KMnO_4$ turned brown. Once the formation of MnO_2 sheets was completed, the brown colloidal aqueous phase was decanted from the organic phase. Colloidal solution was retained in the flask and

reheated to 90^{O}C where it was held for 7 days where it formed into "fluffy" black α-MnO_2. The solution was then washed with ethanol and centrifuged at 10,000 RPM. The washing process was repeated two more times after which the nanowires were dispersed in ethanol.

Confirmation of the α-MnO_2 nanowires was carried out using TEM, SEM and XRD spectroscopy (Figure 11). The synthesis produced needle like wires of lengths between 0.5 – 5 μm and widths between 10 – 20 nm (Figure 11a-b). XRD spectroscopy revealed characteristic peaks of α-MnO_2 confirming the phase of the crystal formed from δ-phase nanosheet to the α-phase nanowire.

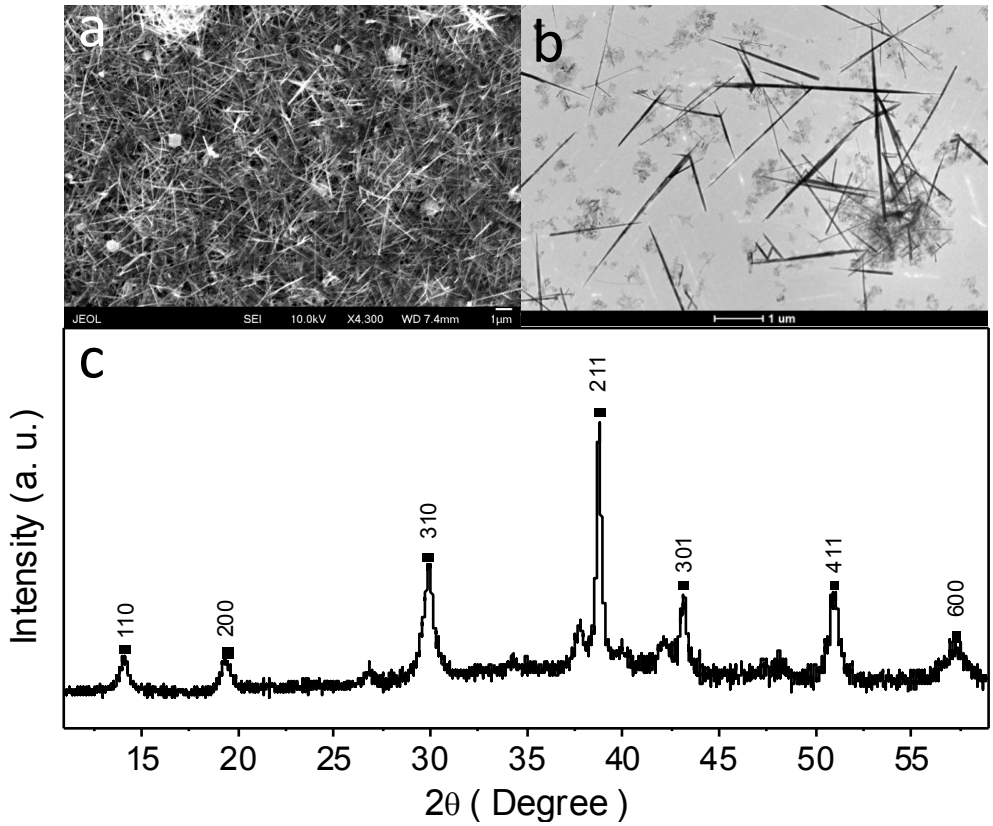

Figure 11 a-b: a) Scanning electron micrograph of α-MnO_2 nanowires. b) Transmission electron micrograph of α-MnO_2 nanowires with length of 500nm – 5 μm with a width ~10-20 nm. c) XRD pattern of α-MnO_2 wires. Nanowires were synthesized following procedure by Sinha et al.[42]

2.2.4 Gold Sputter

Gold sputter deposition was also employed to introduce gold nanoparticles into our electrode. Sputter deposition is a method of depositing a thin film of atoms, from a metal target, on to a substrate by inducing an electric field ejecting atoms into a plasmatic phase where they deposit due to the atoms thermodynamic instability in the plasma

phase. An Anatech Hummer 6.2 sputter coater with a Au target was used to sputter gold on to our electrodes in an argon atmosphere at 75 mTorr and current of 12 milliamperes. The resulting thin film was visible as a purple-blue hue to the electrode (Figure 12 b-d). EDAX was performed

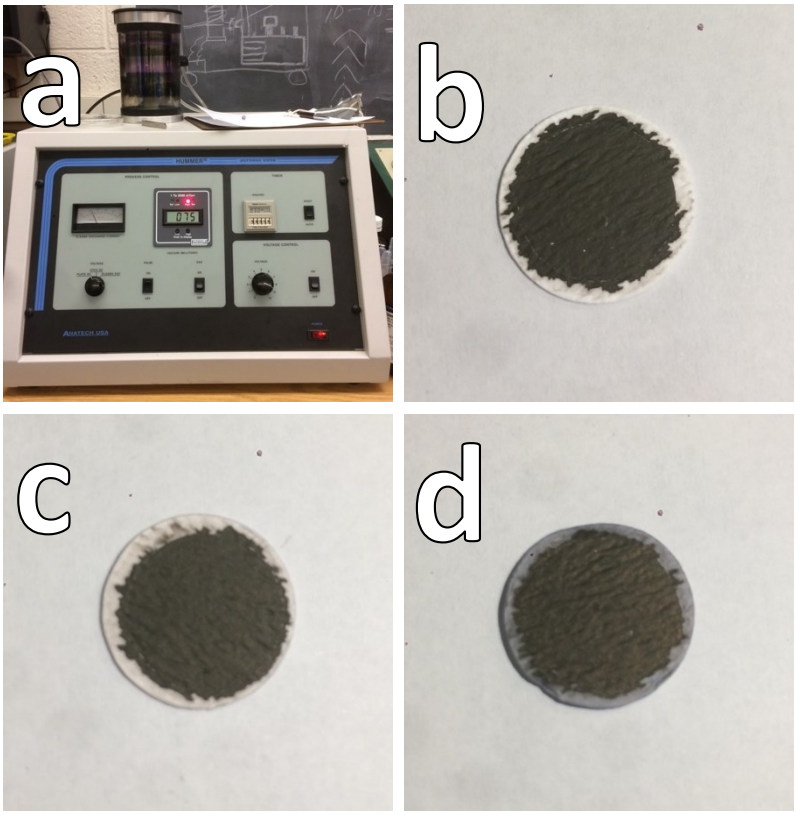

Figure 12 a-d: a) Anatech USA Hummer 6.3 sputter system with Au target. **b)** As prepared vacuum deposited cathode. **c)** Vacuum deposited cathode with 30s of Au sputtering. **d)** Vacuum deposited cathode with 120s of Au sputtering.

Chapter 3: The carbon-based oxygen-breathing cathode

3.1 Introduction

The O_2 cathode is the lungs of an Li-O2 Air battery. During discharge oxygen enters (breathes in) into the cathode where it is reduced, ORR, to LiO_2 and Li_2O_2. On charge, Li_2O_2 is oxidizes and decomposes directly into O_2, OER, and leaves the cathode surface (breathes out). An ideal cathode should have the following properties: offer transport channels for fast oxygen diffusion; provide a three phase (electrolyte/cathode/oxygen) interphase; and adequate void space for the formation of discharge products. Construction of air cathodes generally include a mixture of catalyst (to increase ORR/OER activity), carbon (for high surface area substrate and gas diffusion), and binder. Carbon fiber paper and CNT arrays offer a great backbone for an O_2 breathing cathode. We constructed two different sets of cathodes, the using commercial available carbon paper as support substrate and the second using a binder free CNT array.

3.2 Carbon Fiber Paper Based Cathode

The construction of the carbon fiber paper based cathodes followed a simple and highly reproducible method. To prepare the electrode for nanoparticle deposition, carbon fiber paper (purchased from Fuel Cell Earth) was punched to a diameter of 19 mm and washed in a sonicating bath with toluene for 20 minutes. The toluene was poured off and the carbon fiber paper was washed in hexanes for 20 minutes. The washing step removes dust and other small particles that may contaminate the electrode. After the second wash

the electrode was dried in the antechamber of a glove box overnight. To deposit the electrocatalyst, nanoparticles were dispersed in chloroform at a desired concentration in a scintillation vile and a piece of carbon fiber paper was added to the solution. The scintillation vile was then sonicated for 1 hour. A 2.5 mg/ml solution reproducibly yielded 0.2mg of nanoparticle deposited on the carbon fiber paper. Figure 13, shown below, shows the difference between the nanoparticle deposition performed in hexanes versus chloroform. When hexanes is employed for ultrasonic deposition the Au nanoparticles tend to aggregate forming Au deposits of ~2-3 μm. Ultrasonic deposition in chloroform produced a highly dispersed coating of Au nanoparticles. After ultrasonic deposition, the carbon-fiber-paper/Au np electrode was annealed at 185^{o}C in air for 15 hours to remove the surfactants from the surface. Scanning electron microscopy was employed (Figure 13 d-e) to verify that aggregation of the nanoparticles did not occur.

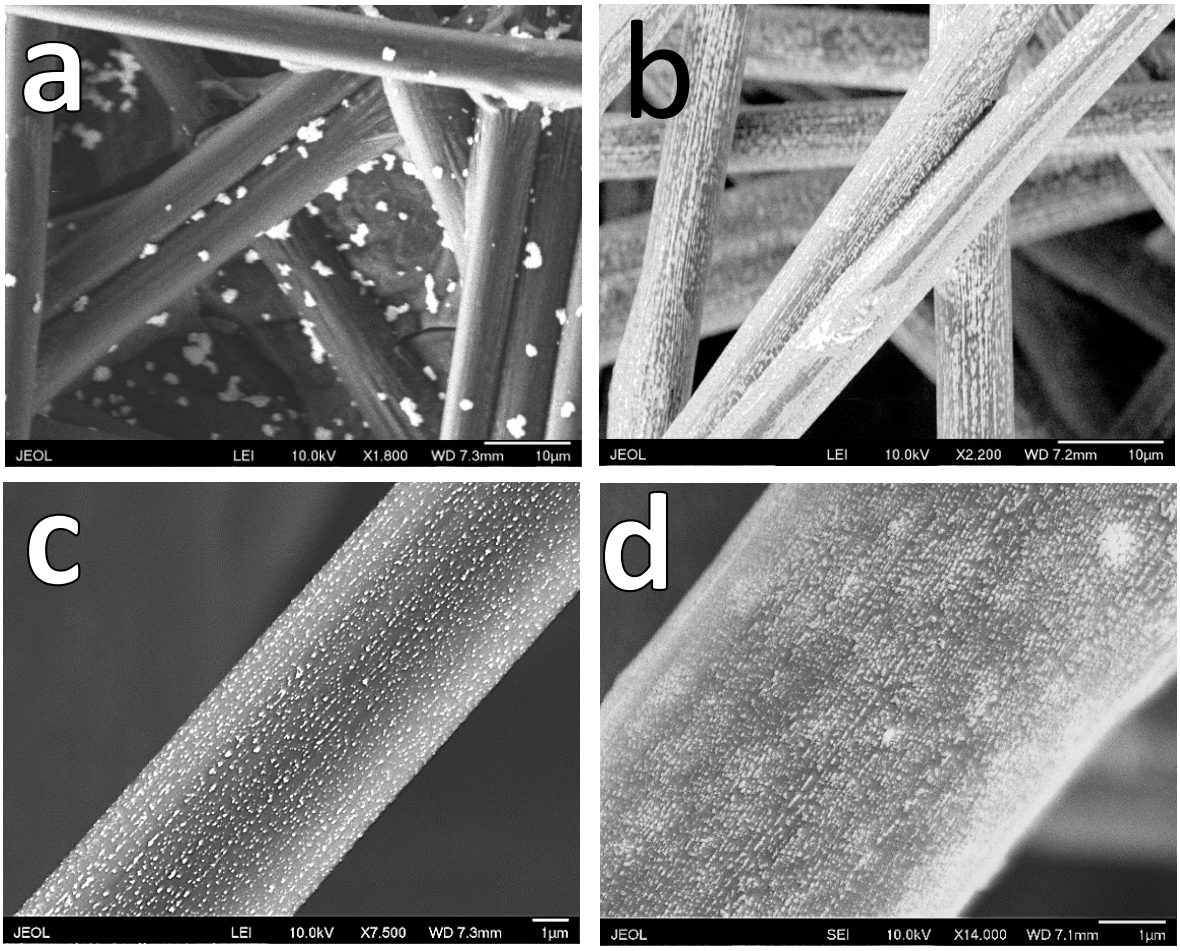

Figure 13 a-d: Image 15 nm Au nanoparticles attached on carbon fiber paper through ultrasonic deposition using (a) hexanes (b) chloroform as a dispersant. (c) SEM image of Au deposited carbon fiber paper before annealing at 185ºC. (d) SEM image of Au deposited carbon fiber paper after annealing at 185ºC

Gold nanowires were also deposited on carbon fiber paper; however, due to inconstant loading during ultra sonic deposition, a drop casting method was used. Drop casting has the benefit of enhance control over nanoparticle loading. A precise measurement of solution can be made and deposited on the electrode surface; though a

major draw back is the wires do not penetrate the electrode very well creating a webbed network on the surface (figure 14a). The use of gold nanowires had to be abandoned, however, due to their high thermal instability. When the drop casted carbon-fiber-paper/Au-nanowire electrode was subjected to annealing at 185^{o}C the unfavorable wire morphology decomposed to nanoparticles (Figure 14b).

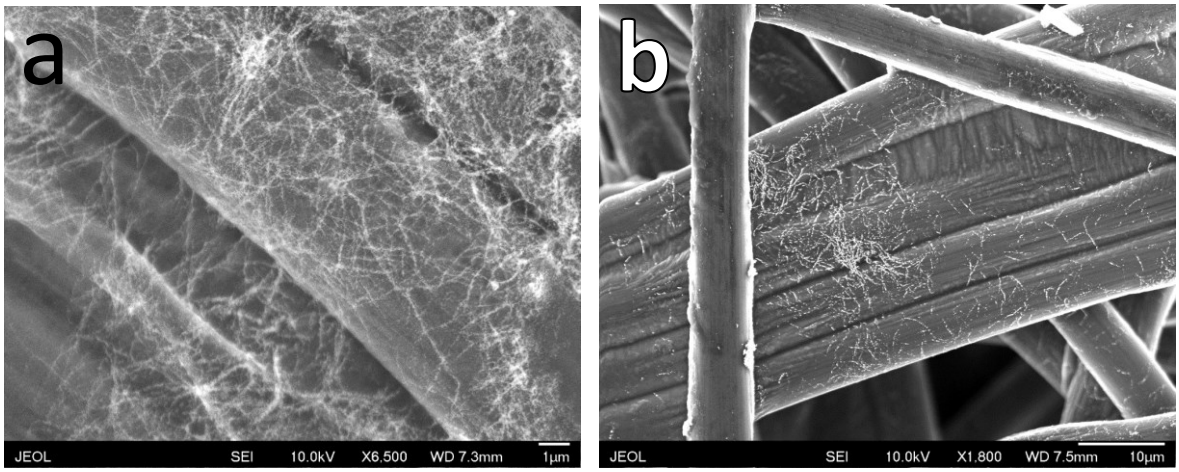

Figure 14 a-b: a) SEM image of Au-nanowires drop cast onto carbon fiber paper creating webbed network on surface of electrode. b) SEM image of Au- nanowire electrode post after annealing at 185^{o}C showing decomposition of wire structure for the favorable nanoparticle morphology.

3.3 Binder-Free Cathode

The advantage of a binder free electrode is three fold. First, most binders are nonconductive, inhibiting electrical connections between the conductive components, thus leaving out the binder will dramatically increase the conductivity and lower the ohmic drop of the electrode. Secondly, binder material flows in to the empty spaces in electrodes blocking the pores and gas passageways that are essential to oxygen diffusion. Once again the absence of the binder will allow for free passage of oxygen throughout the entire electrode. Lastly, discharge products form on the surface of the carbon and electrocatalysts which get masked by binder material. The absence of binder allows greater exposure of the surface and electrocatalyst for discharge product formation.

Electrode Fabrication

A binder-free electrode was developed using single walled carbon nanotubes (SWCNTs or CNTs) and electrocatalyst nanoparticles. The CNTs are used to increase the conductivity and mechanical stability of the electrodes; while the electrocatalysts are used for decreasing the energy barriers of the OER and ORR reactions. The developed method employed a water dispersion of CNTs as well as dispersed electrocatalytic nanowires as cathode materials, which were deposited using vacuum filtration on to a glass-fiber separator substrate (Figure 15). The resulting cathode + separator creates an excellent electrode that combines the large electrolyte wettability of the glass fiber and high volume gas diffusion electrode of the CNT/nanowire array.

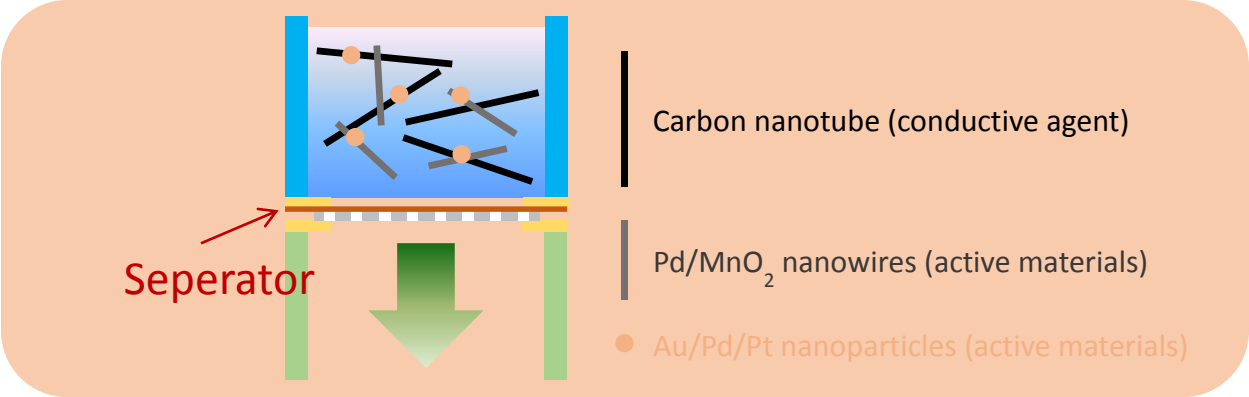

Figure 15: Schematic of cathode material deposition on to glass fiber filter paper using vacuum filtration. Black bars represent CNTs; Grey bars represent electrocatalytic nanowires; orange circles represent other electrocatalytic nanoparticles.

Commercially produced single walled carbon nanotubes (CNTs) (purchased from US Research Nanomaterials) in a 1wt% water dispersion with an average length of 5-30 μm and an OD of 1-2 nm was mixed with the synthesized α-MnO_2 nanowire dispersion to create an α-MnO_2/CNT mixture of 80/20 wt%, 70/30 wt%, or 60/40 wt% (Figure 16c). The α-MnO_2/CNT dispersion was ultrasonicated for 1 hour in 45 ml of ethanol to ensure proper homogenization. GF75 glass fiber filter paper with 0.3 μm pores (manufactured by Advantec) was punched to 19mm in diameter. The filter paper was washed and solicated for 20 minutes in toluene, then twice more in ethanol. The washing and sonication of the glass fiber separators removed free glass fibers, dust, and other contaminates.

To fabricate the electrode a clean glass fiber membrane was placed on standard vacuum filter and was masked by aluminum foil with a 15mm round punch. The bell reservoir of the vacuum filter was placed over the mask and clamped down to ensure a good seal. The reservoir was filled with the α-MnO_2/CNT mixture and filtered through the glass fiber membrane. The sides of the reservoir were sprayed during the filtration process to ensure all the material was deposited on the membrane. While still under vacuum, the electrode was washed with ultrapure 18.2 MΩ Di water to remove residual surfactants. The electrode was then dried in a vacuum over at 80^{o}C for 24 hours. SEM was performed to image the electrode surface (Figure 16a-b). Lower magnifications revealed a strong boundary between glass fiber and deposited cathode material providing strong evidence of negligible material loss during the deposition process. When the magnification was increased to 7000x the α-MnO_2 nanowires could easily be observed as evenly deposited throughout the glass fiber surface.

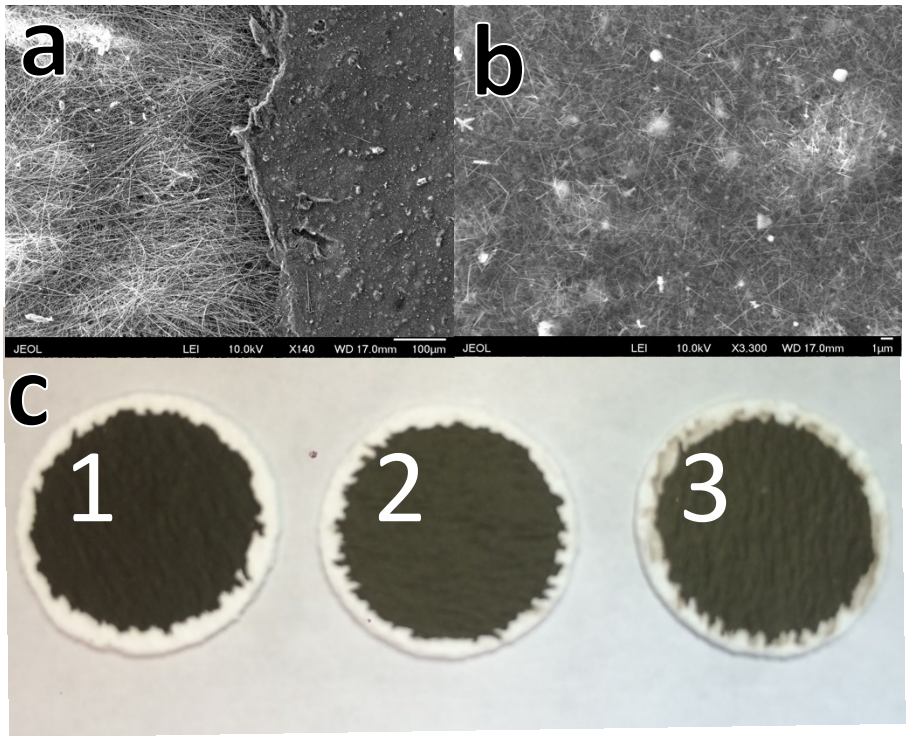

Figure 16 a-c: a-b) Scanning electron micrographs of vacuum deposited α-MnO_2/CNT cathode material on glass fiber substrate. c) 1mg of cathode material deposited on glass fiber substrate w/ α-MnO_2/CNT mixtures of (1) 80/20 wt%, (2) 70/30 wt%, and (3) 60/40 wt%

Chapter 4: Electrochemical Cycling and Testing

4.1 Introduction

Our carbon-fiber-based and binder-free electrodes were subjected to electrochemical cycling and testing to characterize the performance of our electrodes. Galvanostaic cycling was our most used method for testing the cells. Galvanostatic cycling assesses the overall performance of the cell by applying a constant current and measuring the voltage response during charging and discharging. The voltage response is dependent on the state of charge, which is related to the capacity of the battery. Analysis of the voltage profile can give great insight into the different reaction potentials in the battery. Li-O_2 batteries have characteristic charge/discharge plateaus around 4.0v and 2.6V respectively. Galvanostatic cycling was performed using a twenty channel Arbin Instruments BT-2043 Battery Tester with a +/- 10V voltage range, and 100mA Maximum current (Figure 17a). Once the battery fails, it is disassembled in a glove box and prepared for postmortem characterization. Scanning Electron Microscopy (SEM) was performed on a JEOL JSM-6700F Field Emission Scanning Electron Microscope capable of secondary electro imaging and back scattering. X-ray diffraction (XRD) patterns were collected on a PANalytical X'Pert^3 Powder X-Ray Diffractometer equipped with a Cu Kα radiation source (λ=0.15406).

4.2 Li-O_2 Cell Construction

The assembly of the Li-O_2 cell was performed in an argon filled MBraun UNILAB Workstation glove box with gas purification maintained < 1 ppm of H_2O and O_2. The glove box is fitted with a ball valve controlled gas line inlet and outlet for

charging the batteries with oxygen. The Li-O_2 cells were constructed using a STC-Li-Air Split cell, purchased from MTI Corp. (Figure 17b). To assemble the cells, a stainless steal spacer was placed on the compression spring provided with the split cell followed by the Li metal anode. Prior to placement on the stainless spacer the lithium anode was polished to a bright sheen in order to expose fresh lithium metal and removing any oxide layer that may have formed. Next, a clean 19mm diameter glass fiber separator was placed over the lithium anode followed by the carbon-fiber-paper or binder-free cathode. 0.3 ml of electrolyte was then dripped over the surface of the cathode wetting the cell. A nickel foam current collector (purchased from MTI corp.) punched to 19mm in diameter was then placed over the fiber electrode (Figure 17d). The cell was sealed with 4 hex-nuts and hooked up to the ball valve controlled gas line supplying high purity O_2 (purchased from AirGas). The cell was purged with O_2 at 15 psi for 15 minutes after which, the exhaust valve was closed and the cell was charged for more 5 minutes. The cell was then taken out of the glove box for galvanostatic cycling or EIS characterization (Figure 17c).

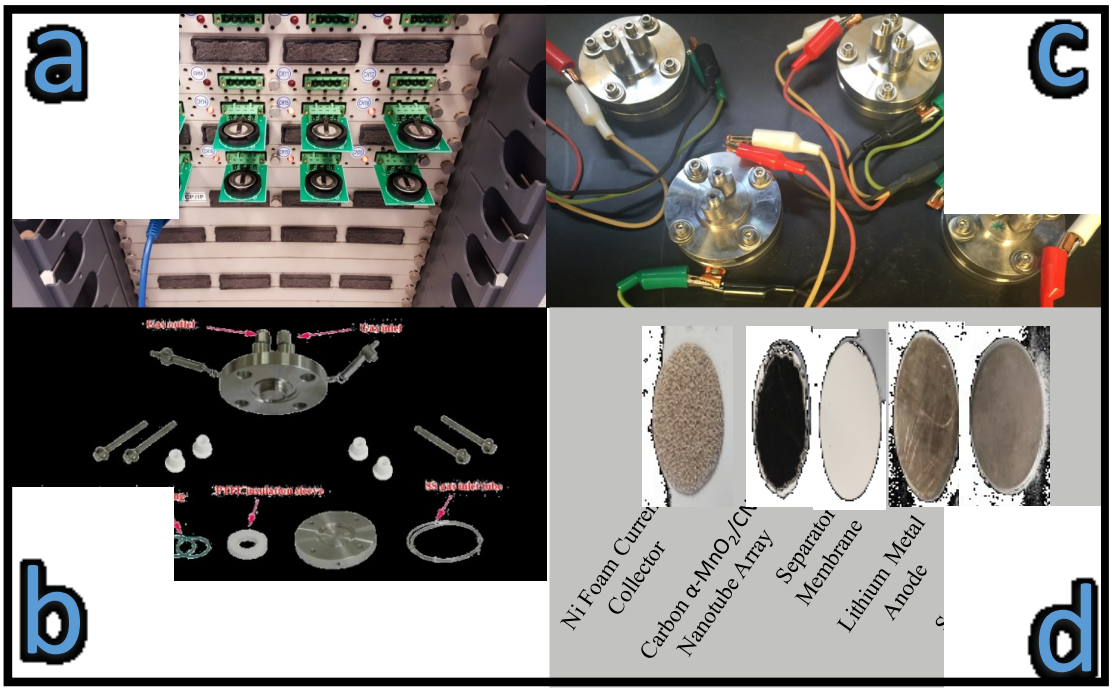

Figure 17 ***a-d:*** a) Arbin Instruments BT-2043 Battery Tester with a +/- 10V voltage range, and 100mA Maximum current. b) Blow up schematic of STC-Li-Air Split cell, purchased from MTI Corp. c) STC-Li-Air Split cell, purchased from MTI Corp connected to Arbin battery tester. d) Internal components Li-O_2 Battery

4.3 Electrochemical Testing of Carbon-Fiber-Paper based Li-O_2 Cells

Our first set of cells were constructed using Li metal anodes, 1M DMSO/$LiCl_4$ electrolyte (purchased from Sigma-Aldritch), and neat carbon fiber paper electrodes, as prepared above, to create a baseline measurement of capacity and cycling performance. The cells were tested using galvanostatic cycling at current density of 10 mA/cm^2 and voltage cut offs of 2V/4V for charge and discharge respectively. Initially, cells were

cycled for a single discharge to evaluate the discharge plateau and capacity of a fresh electrode. 10 cycle tests were also performed to evaluate the cycle life and capacity fade of the batteries.

A representative single discharge profile (Figure 18a) has a discharge at ~2.7 V. When cell voltage hits 2.5V the voltage drops precipitously forming and "elbow" shaped discharge curve. More then 95% of the capacity is discharged before the elbow. Postmortem examination after single discharge using SEM (Figure 18b) reveals the initial formation and nucleation sites of the Li_xO_2 discharge products on the surface of the carbon fibers.

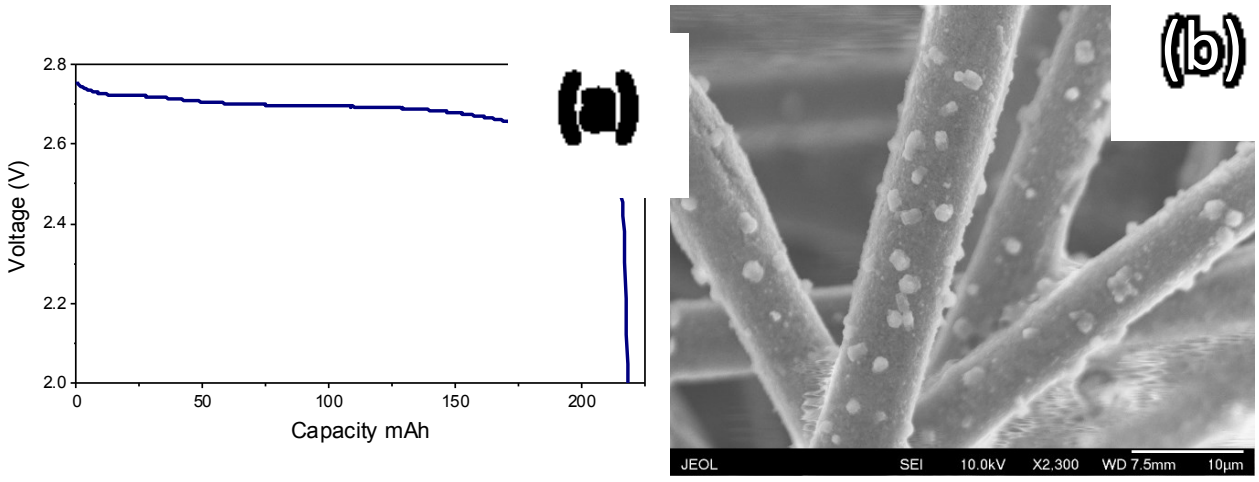

Figure 18 a-b: (a) Capacity vs Voltage profile for the first discharge of an Li-O_2 cell using carbon-fiber-paper electrode. (b) SEM image of carbon-fiber-paper electrode after a single discharge. Discharge products grow as nodules on fresh electrodes.

Neat carbon-fiber-paper based cells were tested for cycle life and capacity retention (Figure 19a). Significant capacity fade is exhibited during cycling with more than 60% lost between first and second cycle and 90% capacity loss by the 5th cycle. These cells also exhibit very poor round trip efficiency of ~55% for the first cycle and decaying to <40% by the 5th cycle. Postmortem analysis using SEM (Figure 19b) revealed a large build up of irreversible discharge product on the carbon fiber surface blocking O_2 passage and masking the electrode surface. This build up of irreversible is in agreement of the before mention literature that states the electrolyte will decompose when in contact of carbon electrodes.

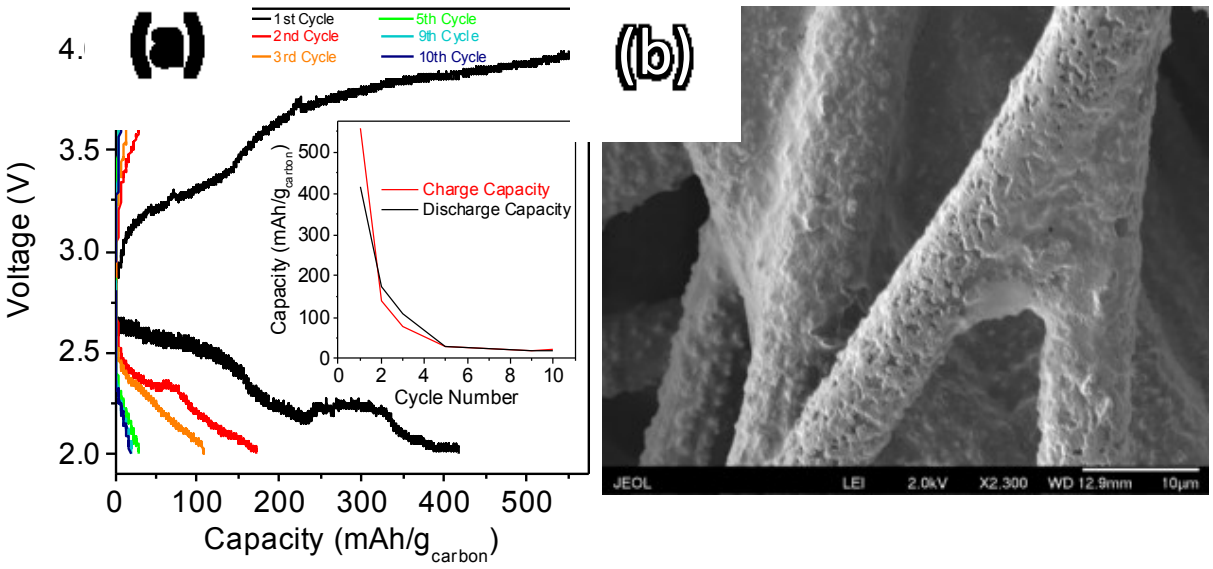

Figure 19 a-b: (a) Voltage vs capacity plot of neat carbon-fiber-paper after 10 discharge/charge cycles. Inlay shows charge and discharge capacity on a per cycle basis. (b) SEM image of post-cycled carbon fiber paper cathode after 10 cycles. Irreversible discharge products deposit as scaly coating causing pore clogging, capacity fade and battery failure.

As previously discussed Shao-Horn et al. demonstrated the benefits of gold electrocatalysts on the discharge performance in Li-O_2 batteries.[24,38] We set out to investigate the performance for ourselves using our carbon-fiber-electrodes with ultrasonically attached 15nm Au nanoparticles. Multi-cycle galvanostatic testing was performed to see the performance and cycling behavior of the cells. The cycling protocol followed the same parameters as the cells built with the neat carbon-fiber-paper based cells.

The addition of gold nanoparticles showed a significant increase in discharge capacity, and round trip efficiency (Figure 20a). The maximum capacity reported for a single cycle was ~1010mAh/g_{carbon}. In addition, the discharge plateau increased to 2.6V from the 2.3V plateau of the neat carbon-fiber-electrode. Postmortem SEM was once again employed to characterize the electrode surface and failure mechanism (figure 20b/c). SEM imaging revealed the build up and clogging of pores by irreversible discharge products was once again the likely cause of failure. Additionally, back scatter imaging revealed the loss of Au nanoparticles from the electrode surface. It's unclear if the particles were unstable in the electrolyte, thus decomposing, or if the adhesion between the Au nanoparticles and carbon fiber surface was not strong enough, detaching the nanoparticles during the formation and loss of reversible discharge products. Thus with this revelation, further investigation of carbon fiber paper based electrode was abandoned for a more mechanically stable CNT/electrocatalytic nanowire arrays.

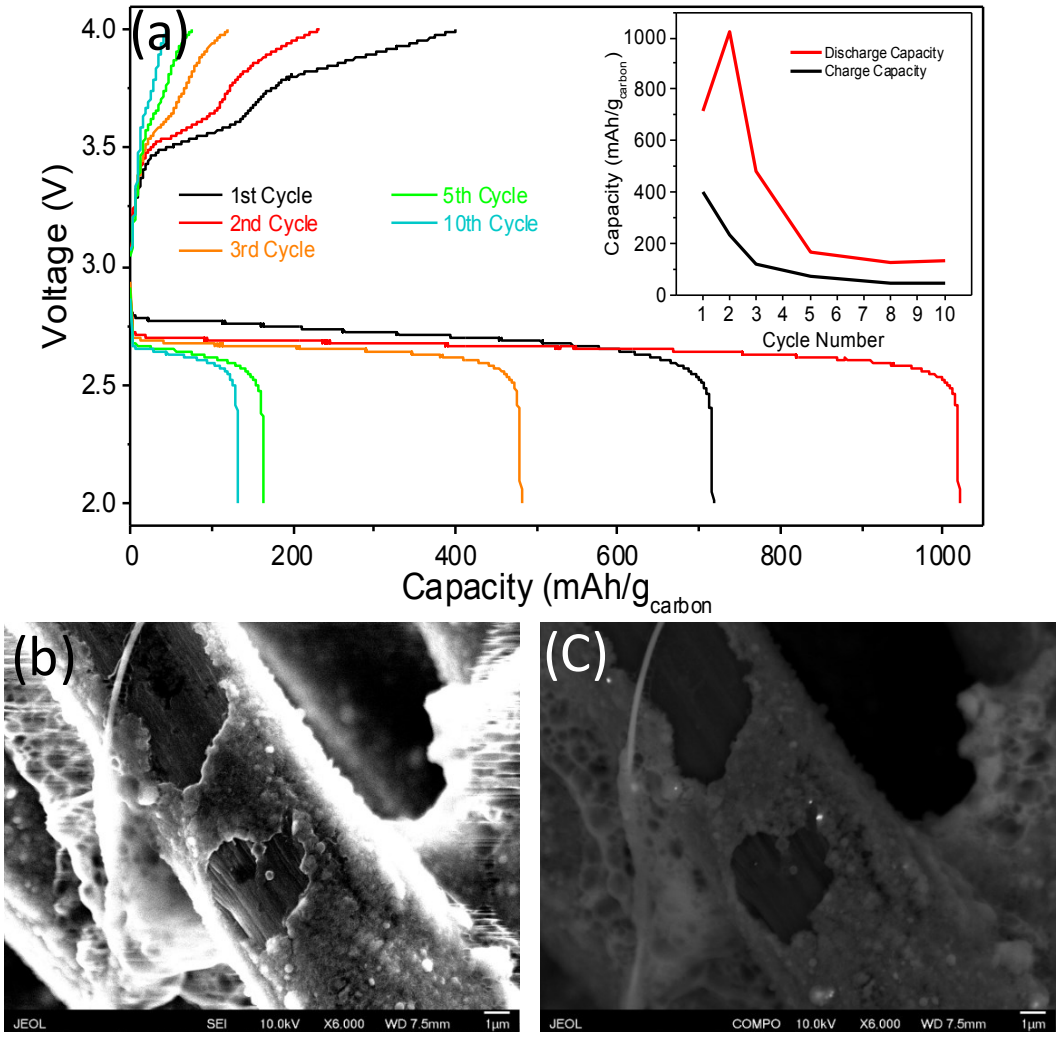

Figure 20 a-c: a) Voltage vs capacity plot of neat carbon-fiber-paper after 10 discharge/charge cycles. Inlay shows charge and discharge capacity on a per cycle basis. b/c) SEM images using the secondary electron imaging (b) and backscattering (c) to detect the presence of Au nanoparticles on carbon fiber paper electrode surface after 10 cycles. Back scattering show loss of Au carbon fiber surface.

4.4 Electrochemical Testing of Binder-Free Electrodes

Due to the adhesion problem experienced with the carbon-fiber-paper based electrodes, our attentions shifted towards the binder-free electrodes mentioned in Chapter 3.3. The cells were tested using two sets galvanostatic cycling parameters. The first set of parameters were voltage limited; a current density of 50 $mA/g_{caothode}$ was applied to the cell with cutoff voltages of 2/4.2V on charge and discharge respectively. The second set of parameters employed capacity limited cycling of 500 $mAh/g_{cathode}$ with a current density of 50 $mA/g_{caothode}$ and voltage cut offs at 1V/5V on discharge and charge respectively.

Our first set of binder-free cells were constructed with Li metal anodes, 70/30 wt.% α-MnO_2/CNT vacuum deposited glass fiber electrode, and DMSO/$LiCl_4$ electrolyte and cell was cycled using voltage limited parameters. The OCV for the cell was quite high at 3.3V compared to the carbon-fiber-paper based electrode's of 2.7V. However, the cycling performance was very poor exhibiting discharge capacities <10 $mAh/g_{cathode}$ (Figure 21).

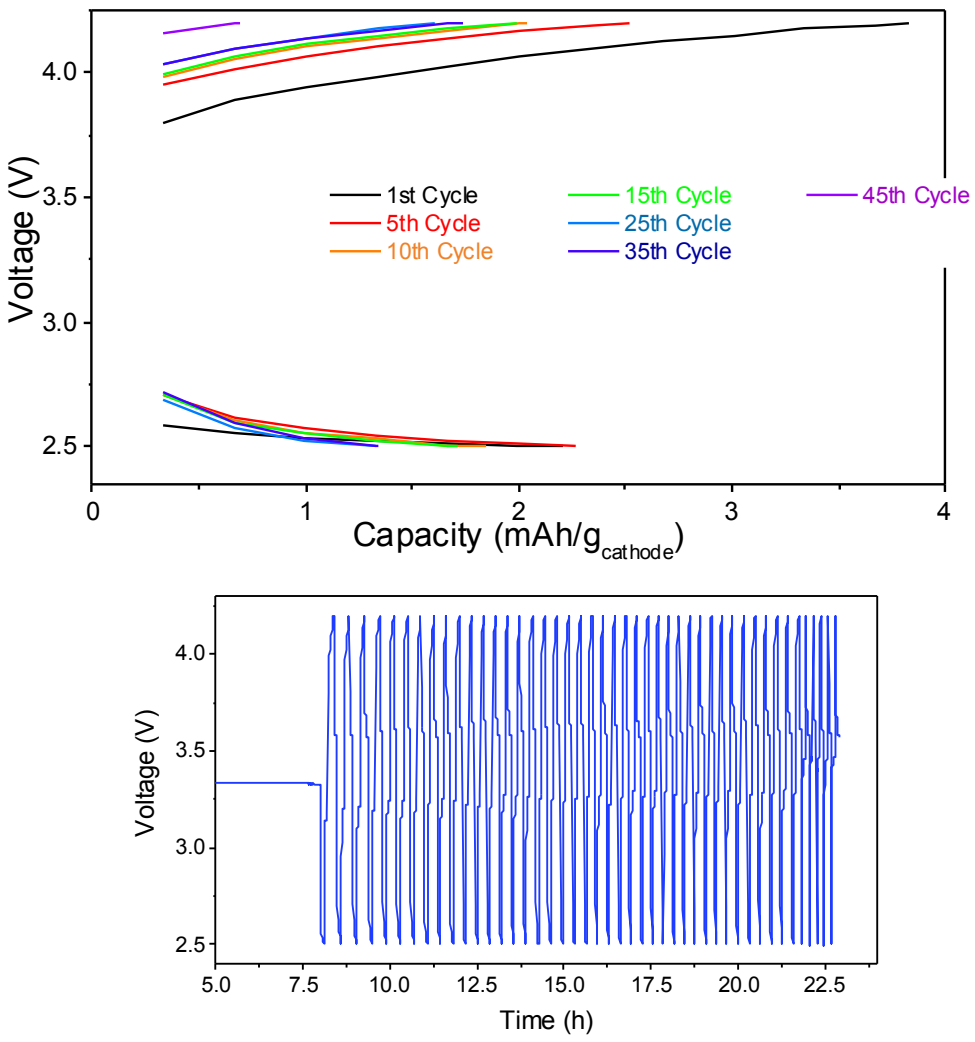

Figure 21: Voltage profile of selected cycles (a) and voltage cycling profile (b) for Li-O_2 cell with Li metal anode, 70/30 wt.% α-MnO_2/CNT cathode, and DMSO/$LiCl_4$ electrolyte. The cell was cycled at 50mA/$g_{cathode}$ with voltage cutoff limits at 4.2V/2.5V on charge/discharge respectively.

In a paper by Bruce et al.[36] showed a carbonate based $LiPF_6$ electrolyte showed excellent performance with α-MnO_2 electrocatalysts. Thus, our next set of batteries used the same construction as previously with the substitution of 1.0 M Lithium hexafluorophosphate in 50/50 vol% ethylene carbonate and diethyl carbonate (EC-DEC/$LiPf_6$, purchased from Sigma-Aldrich) as an electrolyte. The new electrolyte dramatically enhanced the performance of the cell giving a 200x increase in capacity as well as a significant improvement of round trip efficiency (Figure 22).

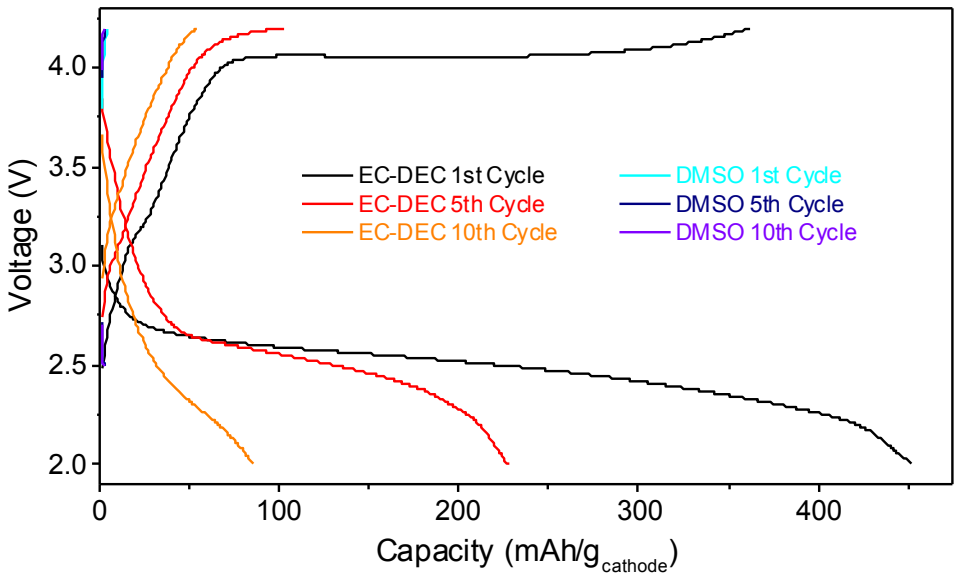

Figure 22: Voltage profile of selected cycles comparing EC-DEC/$LiPF_6$ vs. DMSO/$LiCl_4$ electrolytes in Li-O_2 cell with α-MnO_2/CNT cathode and Li metal anode. The cells were cycled at 50mA/$g_{cathode}$ with voltage cutoff limits at 4.2V/2V on charge/discharge respectively.

The new electrolyte proved to dramatically enhance the capacity and cycle life of our binder-free electrodes over the DMSO/$LiCl_4$ electrolyte based cells and the carbon fiber based paper based cells. Our best performing Li-O_2 cell based on the 70/30 wt.% α-MnO_2/CNT electrode, and EC-DEC/LiLiPF_6 electrolyte cycled for more then 20 cycles before losing 80% of its capacity compared to 5 cycles with the carbon fiber paper based cells. This cell also exhibited very high discharge capacity achieving multiple cycles above 1000 mAh/$g_{cathode}$ (Figure 22).

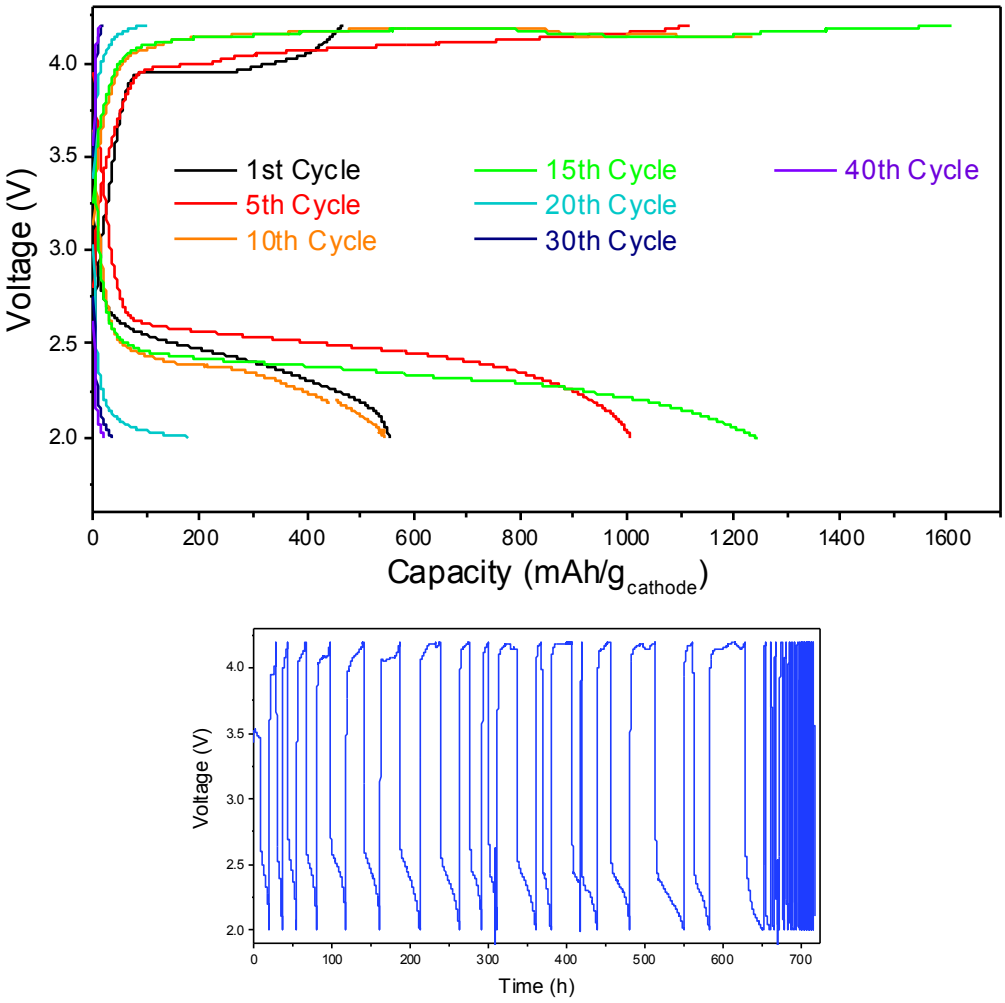

Figure 23: Voltage profile of selected cycles (a) and voltage cycling profile (b) for Li-O_2 cell with Li metal anode, 70/30 wt.% α-MnO_2/CNT cathode, and EC-DEC/LiLiPF$_6$ electrolyte. The cell was cycled at 50mA/$g_{cathode}$ with voltage cutoff limits at 4.2V/2.0V on charge/discharge respectively.

Postmortem characterization was performed on cells to determine the discharge products and give insight into the failure modes of the cells. XRD was performed on 70/30 wt.% α-MnO_2/CNT cathodes before and after cycling. The postmortem XRD pattern shows the presence of both Li_2O_2 and LiO_s in the electrode. In addition, there are additional strong peaks at 45° and 27° 2θ which could not be identified. It is reasonable to believe these peaks represent other irreversible discharge products. To confirm this hypothesis more advanced characterization methods such as FTIR, among others, would need to be used. SEM was also used to image the surface of the failed electrode. The images revealed large amounts of discharge products cover the entire surface of the electrode as well as clogging the pore space between the glass fiber substrate. The results from XRD and SEM supports the notion that long life cells fail due to clogging of the electrode limiting gas diffusion and void volume for discharge products to form into.

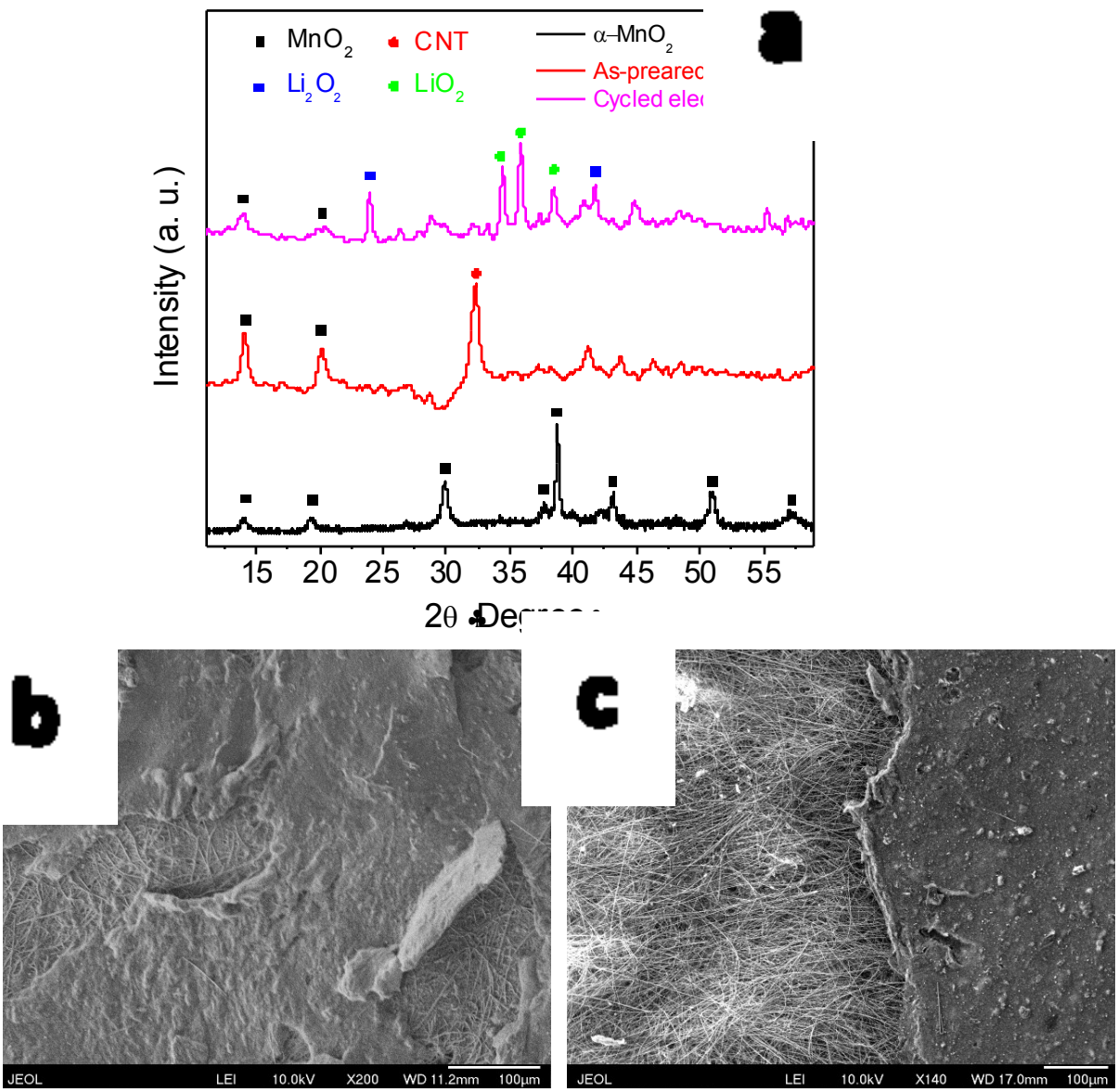

Figure 24 a-c: (a) XRD Patterns of α-MnO_2, pre-cycled as-prepared α-MnO_2/CNT cathode, and post-cycled α-MnO_2/CNT. Post-cycled pattern shows the presence of Li_2O_2/LiO_2 discharge products as well as other unidentifiable peaks. (b-c) SEM image of 70/30 wt.% α-MnO_2/CNT cathode after (b) and before (c) cycling.

Setting a capacity limit of 500 mAh/g based on the weight of the active cathode material allows for longer cycle life by restricting the number of coulombs passed though the electrode, there by limiting the formation of unfavorable and irreversible side reactions. This cycling protocol greatly increase the stability and cyclability of our cells. Multiple cells were constructed demonstrating 50+ cycles at the full capacity of 500 $mAh/g_{caothed.}$. However, it's important to not that that the charge voltage window for cycling does shift to lower voltages as cycle numbers increase, which could be indicative to the cycling occurring at lower states of charge (Figure 25).

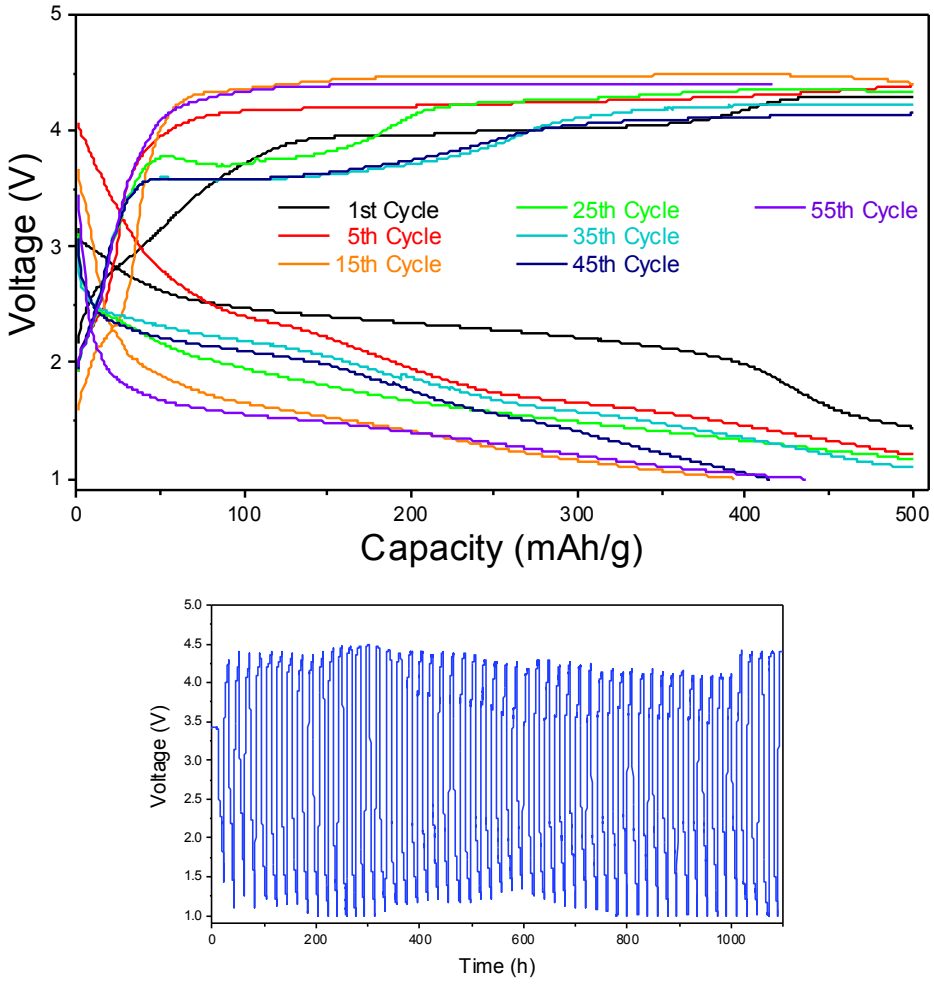

Figure 25: Voltage profile of selected cycles (a) and voltage cycling profile (b) for Li-O_2 cell with Li metal anode, 70/30 wt.% α-MnO_2/CNT cathode, and EC-DEC/LiLiPF$_6$ electrolyte. The cell was cycled at 50mA/$g_{cathode}$ with a capacity limit of 500mAh/$g_{cathode}$ and voltage cutoff limits at 5V/1.0V on charge/discharge respectively.

Ionic liquid electrolytes (ILs) were also employed in our system. Theses electrolytes were explored in a sealed oxygen cell to compliment alternative research into Li-Air batteries being performed in our group. Ionic liquids have the added benefit of having high ionic conductivity and hydrophobicity. The cell was constructed with a Li metal anode, 70/30 wt.% α-MnO_2/CNT cathode, and 1M LiTFSI dissolved in EMIM-TFSI (purchased from EMD Millipre) and cycled using our 500 mAh/$g_{cathode}$ capacity parameters. The cell has performed 29 cycles charge and discharging the limited capacity. Though the voltage window for charge and discharge is large the voltages are holding stable (Figure 26).

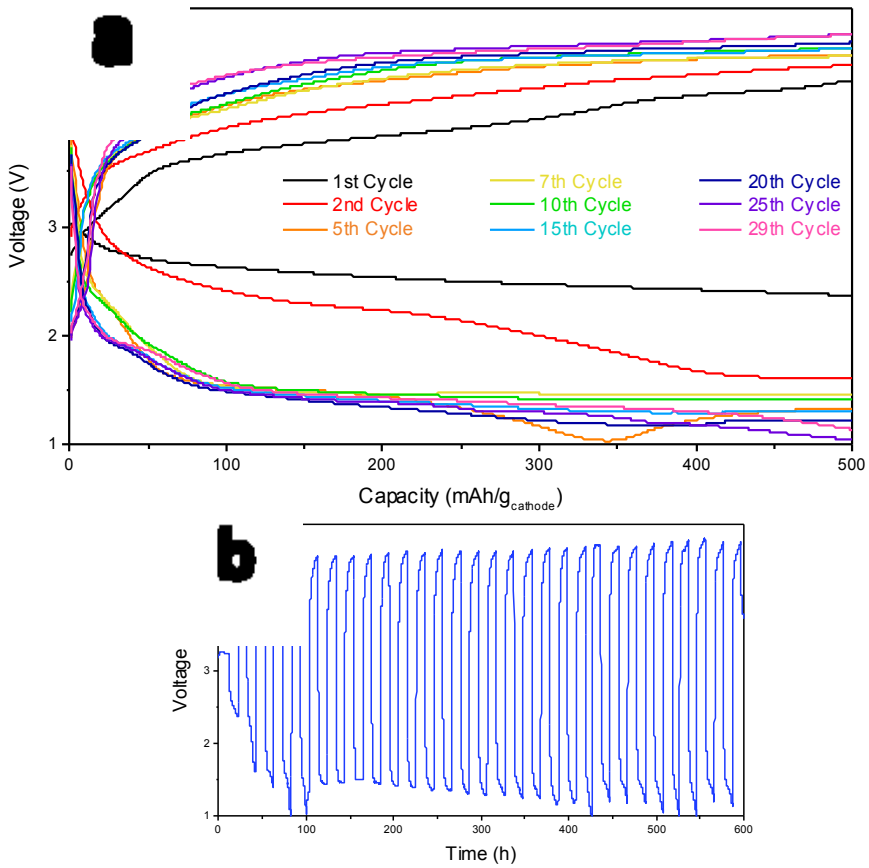

Figure 26: Voltage profile of selected cycles (a) and Voltage cycling profile (b) for Li-O_2 cell with Li metal anode, α-MnO_2/CNT cathode, and EMIM-TFSI/LiTFSI electrolyte. The cell was cycled at 50mA/$g_{cathode}$ with a capacity limit of 500mAh/$g_{Cathode}$ and voltage limits at 5V/1V on charge/discharge respectively.

Sputtering was used to introduce gold into our α-MnO_2/CNT cathodes for use as an electrocatalyst. The α-MnO_2/CNT cathodes with 30s of gold sputtering at 12 milliamperes was cycled using our voltage limited parameter. The cells first discharge had a capacity of ~475 mAh/$g_{cathode}$ with a voltage plateau at an average of 2.6V. The cell performed 10 cycles before 80% of it's capacity was lost. No significant performance enhancement can be noted when comparing the Au sputtered cells to the standard composition cathode (Figure 27b). This result is contrary to the reported literature previously mentioned and to the results we obtained from carbon fiber paper electrodes with ultrasonically deposited 15nm Au nanoparticles.

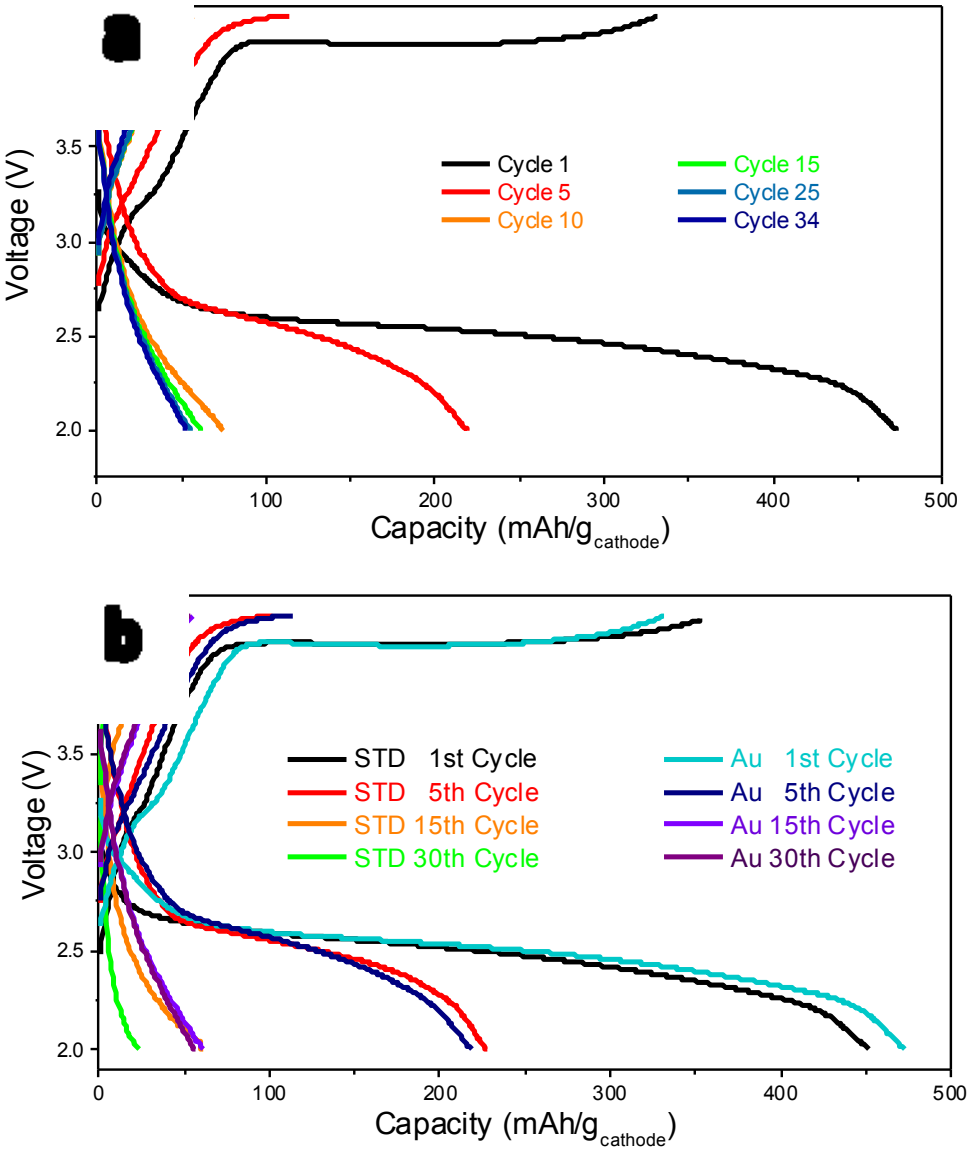

Figure 27 a-b: (a) Voltage profile of selected cycles) for Li-O_2 cell with Li metal anode, α-MnO_2/CNT with 30s of gold sputtering, and EC-DEC/$LiPF_6$ electrolyte. The cell was cycled at 50mA/$g_{cathode}$ with voltage cutoff limits at 4.2V/2V on charge/discharge respectively. (b) Voltage profile of selected cycles comparing Li-O_2 cells with standard α-MnO_2/CNT and α-MnO_2/CNT/Au-sputter cathodes

Chapter 5: Conclusion and Future Directions

As discussed in the introduction, the Li-$O2_2$ battery has the potential to be the "holy grail" of electrochemical energy storage technologies. With a theoretical specific energy comparable to gasoline, the use of Li-O_2 batteries for EVs has significant potential to disrupt the automotive industry. However, many challenges and problems need to be solved for it to be a commercial viable technology. Most notably, the round trip efficiency and cyclability must be dramatically improved to compete with commercial Li-ion batteries which can cycle >500 times at an energy efficiency >90%.[13] The kinetics of the ORR and OER reactions on charge and discharge govern the round trip efficiency, in turn impacting the cycle life. Therefore, improving the air cathodes activities for these reactions can significantly enhance the performance of the battery. This thesis has outlined significant effort into creating new electrocatalytic electrodes to enhance the performance of Li-O_2 batteries.

Our initial attempts at creating a cathode using carbon fiber paper and ultrasonically deposited Au nanoparticles. This cathode combination yielded improved performance of the battery with an 2.5x increase in capacity and 300mV enhancement of the discharge plateau over neat carbon fiber paper electrodes. However, during postmortem analysis with a SEM using backscatter detection reviled the loss of the Au-nanoparticles. Possible reasons for the loss of Au nanoparticles include week adhesion to the electrode surface and particle instability in the electrolyte.

We also developed a vacuum deposition technique for creating a binder free electrode using α-MnO_2 nanowires as a bi-functional electrocatalyst for OER/ORR and single walled carbon nanotubes for conductivity and mechanical support. Li-O_2 cells built with a Li metal anode, 70/30 wt% α-MnO_2/CNT cathodes, and 1M EC-DEC/$LiPF_6$ electrolyte. Our best performing cells were able to perform >50 cycles at a capacity limit of 500 $mAh/g_{cathode}$ with discharge and charge plateaus at 1.5V and 4.3V respectively. When the voltage was limited to 4.2V and 2V for charge and discharge significant capacity loss was observed during cycling with the cells losing 90% of its capacity by the 20^{th} cycle. Postmortem analysis using SEM and XRD reviled significant amounts of discharge product remained in the cathode after cycling and is the most reasonable cause for failure. Discharge products detected using XRD included Li_2O_2, LiO_2, as well as other unidentifiable peaks that were not present on an as prepared cathode. In the future other characterization techniques should be employed to better identify the nature of the discharge products. More robust analysis techniques include FTIR, NMR, Iodometric titration.

Gold sputtered binder free cathodes from 70/30 wt% α-MnO_2/CNT were also cycled. The addition of gold in this form did not have any significant impact on cycling performance. These results are contrary to our initial experiments using carbon fiber paper electrodes with Au nanoparticles and to results published in literature.

Lastly stable cycling was achieved using a 1M EMiM-TFSI/LiTFSI ionic liquid electrolyte in our cells. Ionic liquids have garnered much attention as a potential

electrolyte for Li-Air cells due to their hydrophobicity and negligible volatility. The IL electrolyte provided minimal performance enhancement In the sealed Li-O_2 cell; however, the stable cycling does prove that I has potential to be used in battery that breathes oxygen in from ambient air.

Although the outcome of our research did not yield a significantly improved system over what has been developed elsewhere, we did create a stable system laying the ground work for futures studies to be performed. Most notably, the vacuum deposition of our glass-fiber/CNT/α-MnO_2 electrode allows for the facile integration of other electrocatalysts. Future work should include the addition of other more catalysts in to the system. Due to the inconclusive results obtained from gold sputtering, Au nanoparticles should be added to the cathode solution and tested as an electrode to confirm weather or not gold has any added benefits. Lastly, literature extensively reports the instability of the electrolyte in the presence of a carbon-based cathode. Therefore, it would be interesting to investigate carbon free electrodes such as nanoporous gold or other conductive porous substrates.

Appendices

A1. Free standing CNT electrode

An attempt was made to create a free standing electrodes for use in our Li-O2 battery; however, the loading of CNTs needed to create a mechanically stable electrode made it prohibitive to integrate the MnO_2 nanowires at the desired wt%. A freestanding electrode from pure CNTS was made to demonstrate the potential for construction. To fabricate the freestanding electrode 50 mg of CNTs were vacuum filtered on to a PVDF membrane. The membrane was heated at $70^{O}C$ in a vacuum oven over night. The CNT puck would delaminate from the PVDF membrane creating a mechanically stable freestanding CNT Array (Figure 28) .

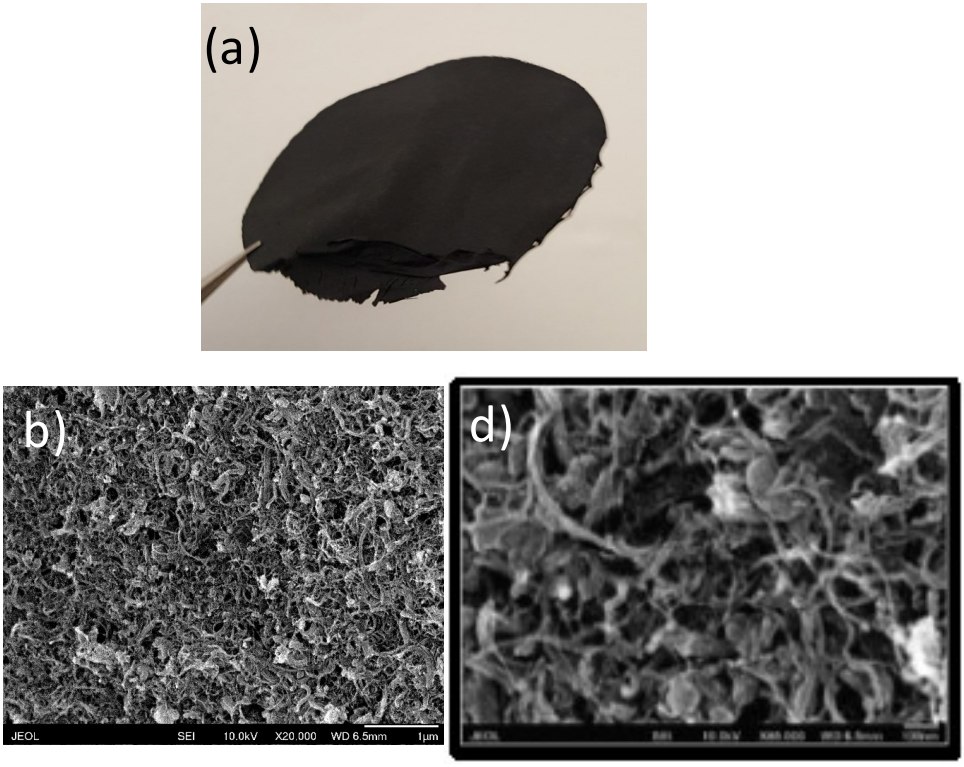

Figure 28: (a) Digital photograph of a freestanding CNT array. Scanning electron micrograph (b) of CNT array under 20,000x magnification, (c) CNT array under 85,000x magnification.

A2. Electrochemical impedance spectroscopy (EIS)

Electrochemical Impedance spectroscopy (EIS) was also employed to test the cell and surface/charge transfer resistance of a few of our cells. During EIS the cell is exposed to a sinusoidal electrical signal over a large range of frequencies. The cell responds to these signals, which can be related to Ohm's Law and give insight to various impedances of the cell. Electrochemical Impedance Spectroscopy (EIS) was performed on an Autolab PGSTAT302N with a FRA32M Impedance Analysis module (Purchased from Metrohm AG). The tests were performed at open circuit potential (OCP) with a frequency range from 100 kHz to 10 mHz with a +/- 5 mV amplitude.

EIS was performed on an uncycled Li-O_2 cell and one that had performed 60 cycles. As is to be expected from long lived batteries, both the cell resistance and charge transfer significantly increased. In this case, by an entire order of magnitude. Nyquist plots for these cells can be found below.

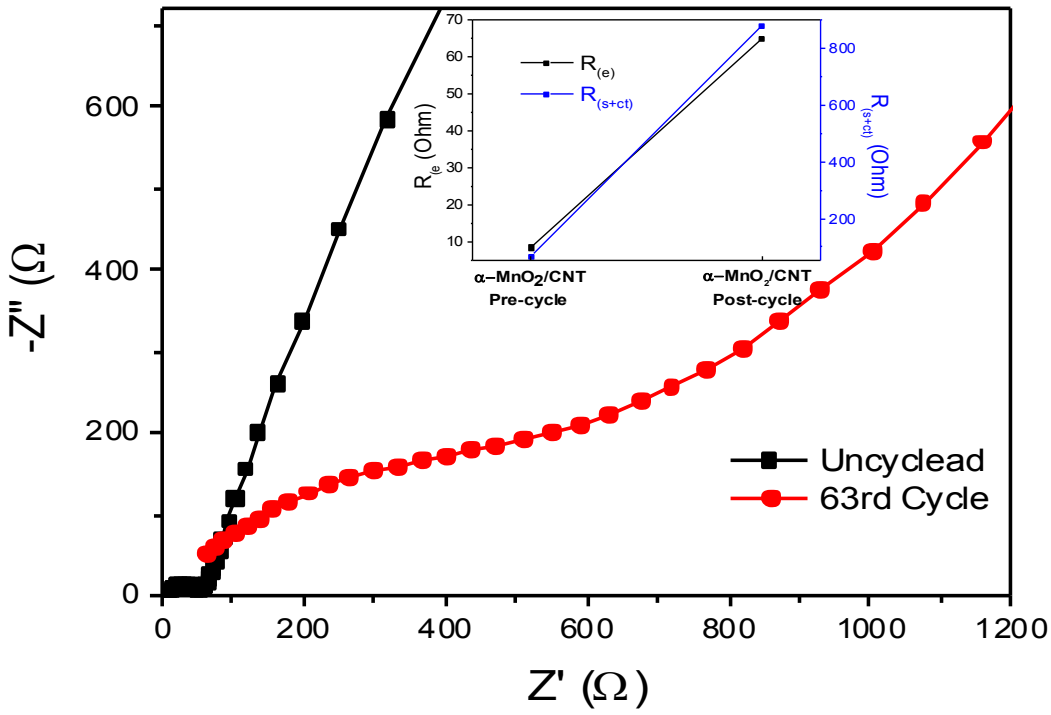

Figure 29: Nyquist impedance plots comparing pre-cycled and post-cycled Li-O_2 cells. Insert panel shows the cell resistance ($R_{e)}$ and the combination of the surface and charge transfer resistances.

EiS was also performed on Li-O_2 cells constructed with standard α-MnO_2/CNT cathodes and α-MnO_2/CNT cathodes with 30s and 120s of gold sputtering. EIS reveiled the gold sputtering increase both the overall sell resistance and charge transfer resistance of the cells. Nyquist plots for all three of these cells can be found below.

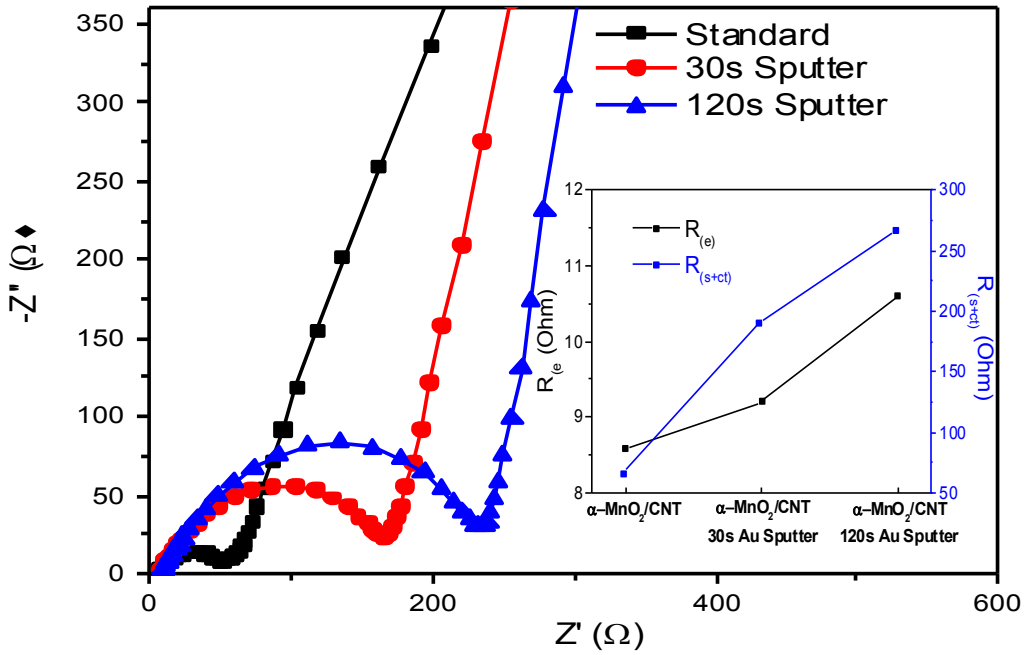

Figure 30: Nyquist impedance plots comparing Li-O_2 cells constructed with cathodes that were gold sputtered for 0s, 30s, and 120s. Insert panel shows the cell resistance (R_e) and the combination of the surface and charge transfer resistances.

List Of References

1 Commission, E. in *Questions and Answers on the European Commission Communication: The Paris Protocol – A blueprint for tackling global climate change beyond 2020* (2015).

2 IPCC. Climate Change 2014: Mitigation of Climate Change. Contribution of Working Group III to the Fifth Assessment Report of the Intergovernmental Panel on Climate Change. (Cambridge, United Kingdom and New York, USA, 2014).

3 Hamilton, K. in *Energy Information Administration Energy Conference.*

4 Carella, C. *London* (Foster & Sullivan, 2015).

5 Li, Y. & Dai, H. Recent advances in zinc-air batteries. *Chem Soc Rev* **43**, 5257-5275, doi:10.1039/c4cs00015c (2014).

6 Bruce, P. G., Freunberger, S. A., Hardwick, L. J. & Tarascon, J. M. Li-O-2 and Li-S batteries with high energy storage (vol 11, pg 19, 2012). *Nat Mater* **11**, doi:10.1038/Nmat3237 (2012).

7 Abraham, K. & Jiang, Z. A polymer electrolyte-based rechargeable lithium/oxygen battery. *Journal of The Electrochemical Society* **143**, 1-5 (1996).

8 Ogasawara, T., Débart, A., Holzapfel, M., Novák, P. & Bruce, P. G. Rechargeable Li2O2 electrode for lithium batteries. *Journal of the American Chemical Society* **128**, 1390-1393 (2006).

9 Imanishi, N., Luntz, A. C. & Bruce, P. *The lithium air battery: fundamentals*. (Springer, 2014).

10 Girishkumar, G., McCloskey, B., Luntz, A. C., Swanson, S. & Wilcke, W. Lithium−Air Battery: Promise and Challenges. *The Journal of Physical Chemistry Letters* **1**, 2193-2203, doi:10.1021/jz1005384 (2010).

11 Lu, Y.-C. *et al.* Lithium–oxygen batteries: bridging mechanistic understanding and battery performance. *Energy & Environmental Science* **6**, 750, doi:10.1039/c3ee23966g (2013).

12 Laoire, C. O., Mukerjee, S., Abraham, K., Plichta, E. J. & Hendrickson, M. A. Influence of nonaqueous solvents on the electrochemistry of oxygen in the rechargeable lithium− air battery. *The Journal of Physical Chemistry C* **114**, 9178-9186 (2010).

13 Wen, Z., Shen, C. & Lu, Y. Air Electrode for the Lithium–Air Batteries: Materials and Structure Designs. *ChemPlusChem* **80**, 270-287 (2015).

14 Hassoun, J., Croce, F., Armand, M. & Scrosati, B. Investigation of the O2 electrochemistry in a polymer electrolyte solid-state cell. *Angew Chem Int Ed Engl* **50**, 2999-3002, doi:10.1002/anie.201006264 (2011).

15 Peng, Z. *et al.* Oxygen reactions in a non-aqueous Li+ electrolyte. *Angew Chem Int Ed Engl* **50**, 6351-6355, doi:10.1002/anie.201100879 (2011).

16 Reddy, T. *Linden's Handbook of Batteries, 4th Edition*. (McGraw-Hill Education, 2010).

17 Tarascon, J.-M. & Armand, M. Issues and challenges facing rechargeable lithium batteries. *Nature* **414**, 359-367 (2001).

18 Freunberger, S. A. *et al.* Reactions in the rechargeable lithium–O2 battery with alkyl carbonate electrolytes. *Journal of the American Chemical Society* **133**, 8040-8047 (2011).

19 McCloskey, B., Bethune, D., Shelby, R., Girishkumar, G. & Luntz, A. Solvents' critical role in nonaqueous lithium–oxygen battery electrochemistry. *The Journal of Physical Chemistry Letters* **2**, 1161-1166 (2011).

20 McCloskey, B. *et al.* Twin problems of interfacial carbonate formation in nonaqueous Li–O2 batteries. *The journal of physical chemistry letters* **3**, 997-1001 (2012).

21 Mizuno, F., Nakanishi, S., Kotani, Y., Yokoishi, S. & Iba, H. Rechargeable Li-air batteries with carbonate-based liquid electrolytes. *Electrochemistry* **78**, 403-405 (2010).

22 Christensen, J. *et al.* A Critical Review of Li/Air Batteries. *Journal of The Electrochemical Society* **159**, R1, doi:10.1149/2.086202jes (2012).

23 Freunberger, S. A. *et al.* The lithium-oxygen battery with ether-based electrolytes. *Angew Chem Int Ed Engl* **50**, 8609-8613, doi:10.1002/anie.201102357 (2011).

24 Lu, Y. C., Gasteiger, H. A. & Shao-Horn, Y. Catalytic activity trends of oxygen reduction reaction for nonaqueous Li-air batteries. *J Am Chem Soc* **133**, 19048-19051, doi:10.1021/ja208608s (2011).

25 Allen, C. J. *et al.* Oxygen Reduction Reactions in Ionic Liquids and the Formulation of a General ORR Mechanism for Li–Air Batteries. *The Journal of Physical Chemistry C* **116**, 20755-20764, doi:10.1021/jp306718v (2012).

26 Mizuno, F. *et al.* Cathode reaction mechanism of non-aqueous Li–O2 batteries with highly oxygen radical stable electrolyte solvent. *Journal of Power Sources* **228**, 47-56, doi:10.1016/j.jpowsour.2012.11.077 (2013).

27 Cui, Z. H., Fan, W. G. & Guo, X. X. Lithium–oxygen cells with ionic-liquid-based electrolytes and vertically aligned carbon nanotube cathodes. *Journal of Power Sources* **235**, 251-255, doi:10.1016/j.jpowsour.2013.02.025 (2013).

28 Chen, Y., Freunberger, S. A., Peng, Z., Barde, F. & Bruce, P. G. Li-O2 battery with a dimethylformamide electrolyte. *J Am Chem Soc* **134**, 7952-7957, doi:10.1021/ja302178w (2012).

29 Peng, Z., Freunberger, S. A., Chen, Y. & Bruce, P. G. A reversible and higher-rate Li-O2 battery. *Science* **337**, 563-566 (2012).

30 Nasybulin, E. *et al.* Effects of Electrolyte Salts on the Performance of Li–O2Batteries. *The Journal of Physical Chemistry C* **117**, 2635-2645, doi:10.1021/jp311114u (2013).

31 Ottakam Thotiyl, M. M., Freunberger, S. A., Peng, Z. & Bruce, P. G. The carbon electrode in nonaqueous Li-O2 cells. *J Am Chem Soc* **135**, 494-500, doi:10.1021/ja310258x (2013).

32 Shao, Y. *et al.* Electrocatalysts for Nonaqueous Lithium–Air Batteries: Status, Challenges, and Perspective. *ACS Catalysis* **2**, 844-857, doi:10.1021/cs300036v (2012).

33 Tran, C., Yang, X.-Q. & Qu, D. Investigation of the gas-diffusion-electrode used as lithium/air cathode in non-aqueous electrolyte and the importance of carbon material porosity. *Journal of Power Sources* **195**, 2057-2063, doi:10.1016/j.jpowsour.2009.10.012 (2010).

34 Mitchell, R. R., Gallant, B. M., Thompson, C. V. & Shao-Horn, Y. All-carbon-nanofiber electrodes for high-energy rechargeable Li–O2 batteries. *Energy & Environmental Science* **4**, 2952, doi:10.1039/c1ee01496j (2011).

35 Lim, H. D. *et al.* Enhanced power and rechargeability of a Li-O2 battery based on a hierarchical-fibril CNT electrode. *Adv Mater* **25**, 1348-1352, doi:10.1002/adma.201204018 (2013).

36 Débart, A., Paterson, A. J., Bao, J. & Bruce, P. G. α-MnO2 Nanowires: A Catalyst for the O2 Electrode in Rechargeable Lithium Batteries. *Angewandte Chemie* **120**, 4597-4600, doi:10.1002/ange.200705648 (2008).

37 Débart, A., Bao, J., Armstrong, G. & Bruce, P. G. An O2 cathode for rechargeable lithium batteries: The effect of a catalyst. *Journal of Power Sources* **174**, 1177-1182, doi:10.1016/j.jpowsour.2007.06.180 (2007).

38 Lu, Y.-C. *et al.* Platinum− gold nanoparticles: A highly active bifunctional electrocatalyst for rechargeable lithium− air batteries. *Journal of the American Chemical Society* **132**, 12170-12171 (2010).

39 Ottakam Thotiyl, M. M. *et al.* A stable cathode for the aprotic Li-O2 battery. *Nat Mater* **12**, 1050-1056, doi:10.1038/nmat3737 (2013).

40 Hiramatsu, H. & Osterloh, F. E. A simple large-scale synthesis of nearly monodisperse gold and silver nanoparticles with adjustable sizes and with exchangeable surfactants. *Chemistry of Materials* **16**, 2509-2511 (2004).

41 Kang, Y., Ye, X. & Murray, C. B. Size- and shape-selective synthesis of metal nanocrystals and nanowires using CO as a reducing agent. *Angew Chem Int Ed Engl* **49**, 6156-6159, doi:10.1002/anie.201003383 (2010).

42 Sinha, A. K., Pradhan, M. & Pal, T. Morphological Evolution of Two-Dimensional MnO2Nanosheets and Their Shape Transformation to One-Dimensional Ultralong MnO2Nanowires for Robust Catalytic Activity. *The Journal of Physical Chemistry C* **117**, 23976-23986, doi:10.1021/jp403527p (2013).

Scholarly Life

Jerome Fineman was born in Berkeley Ca, on September 18, 1984. He graduated from Polytechnic Institute of New York University in 2012 with a Bachelor's in Chemical and Biomolecular Engineering. After his graduation he worked as a Research Associate at City College of New York in the CUNY Energy institute investigating grid-scale energy storage through funding by ARPA-E. In 2014 Jerome entered the Master of Science in Chemical and Biomolecular Engineering program at Johns Hopkins University.